Quaternary Science Reviews 273 (2021) 107248

Contents lists available at ScienceDirect

Quaternary Science Reviews

journal homepage: www.elsevier.com/locate/quascirev

Origins of the divergent evolution of mountain glaciers during deglaciation: Hofsdalur cirques, Northern Iceland

Luis M. Tanarro [a, *], David Palacios [a], José M. Fernández-Fernández [b], Nuria Andrés [a], Marc Oliva [c], Manuel Rodríguez-Mena [a], Irene Schimmelpfennig [d], Skafti Brynjólfsson [e], Þorsteinn Sæmundsson [f], José J. Zamorano [g], Jose Úbeda [a], ASTER Team

[a] High Mountain Physical Geography Research Group. Department of Geography, Universidad Complutense de Madrid, Madrid, 28040, Madrid, Spain
[b] Centro de Estudos Geográficos (CEG), Instituto de Geografia e Ordenamento Do Território (IGOT), Universidade de Lisboa, Lisbon, Portugal
[c] Department of Geography, Universitat de Barcelona, Barcelona, Spain
[d] Aix-Marseille Université, CNRS, IRD, INRAE, Coll. France, UM 34 CEREGE, Technopôle de L'Environnement Arbois-Méditerranée, BP 80, 13545, Aix-en-Provence, France
[e] Icelandic Institute of Natural History, Akureyri, Iceland
[f] Faculty of Life and Environmental Science, University of Iceland, Reykjavík, Iceland
[g] Institute of Geography, Universidad Nacional Autónoma de México, México, DF, Mexico

ARTICLE INFO

Article history:
Received 6 July 2021
Received in revised form
1 October 2021
Accepted 18 October 2021
Available online 2 November 2021

Handling Editor: C. O'Cofaigh

Keywords:
Iceland
Hofsdalur
Tröllaskagi peninsula
Glacial evolution
Debris-covered glaciers
Rock glaciers
Younger dryas
Holocene
Holocene thermal maximum

ABSTRACT

The aim of this work is to study the process of transformation of debris-free mountain glaciers into debris-covered glaciers and rock glaciers, and to examine the factors driving diverging evolution in similar glacial systems. The study area is the Hofsdalur valley, in the Tröllaskagi peninsula (northern Iceland), where several cirques host a great diversity of glaciers and rock glaciers as well as various glacial landforms. Four adjacent cirques have been analysed through a multidisciplinary approach: geomorphological analysis, boulder surface displacement tracking, quantification of recent glacier changes, three dimensional palaeoglacier reconstruction, equilibrium-line altitude calculations and relative and direct dating methods applied to surface boulders. Dating methods included *in situ* ^{36}Cl cosmic-ray exposure dating, Schmidt hammer weathering measurements and lichenometric dating. The results confirm that glaciers in Hofsdalur followed an evolution pattern similar to that observed in other cirques in the Tröllaskagi peninsula. During the Younger Dryas (12.9–11.7 ka) many of those cirques hosted debris-free glaciers, whose retreat started in the early Holocene. Distinct retreat dynamics and cirque floor elevation conditioned the subsequent glacial evolution. In some Tröllaskagi cirques, the ice completely covered the headwalls, which consequently did not supply debris onto the glacier surface, which remained debris-free. In most of these cirques, however, glacier retreat enhanced paraglacial processes and the ice-free cirque walls generated a high debris supply onto the glacier surface. As a result, the glaciers evolved towards debris-covered glaciers or rock glaciers, depending on the local topographical setting. In the lower cirques they collapsed immediately after their formation. At higher altitudes, above the lower permafrost limit, these ice-cored landforms have survived until the present day, but they have been stagnant since the Holocene Thermal Maximum, while the heads of these cirques have hosted debris-free glaciers during the Late Holocene.

1. Introduction

Mountain glaciers of both hemispheres have accelerated their retreat over recent decades (Roe et al., 2017). They have contributed during this time about one-third of the ice melt to the sea level rise (Gardner et al., 2013; Bamber et al., 2018; Herreid and Pellicciotti, 2020). The retreat of mountain glaciers as a consequence of increasing temperatures is parallel to their transformation from debris-free to debris-covered glaciers, as is occurring in the Alps (Deline, 2005), Caucasus (Lambrecht et al., 2011; Tielidze et al., 2020a, 2020b), Himalaya (Shukla et al., 2009; Bhambri et al., 2011; Thakuri et al., 2014; Scherler and Egholm, 2020), Patagonia

* Corresponding author.
E-mail address: pace@ghis.ucm.es (L.M. Tanarro).

https://doi.org/10.1016/j.quascirev.2021.107248

(Glasser et al., 2016), and in the Southern Alps of New Zealand (Quincey and Glasser, 2009). Globally, more than 20% of the predominantly debris-free glaciers have debris-covered sectors, which accounts for 7.3% of mountain glacier area (Herreid and Pellicciotti, 2020). As a continuation of the transformation, the new debris-covered glaciers may end up becoming rock glaciers (Hambrey et al., 2008; Berthling, 2011; Monnier and Kinnard, 2016; Janke et al., 2013, 2015; Rowan et al., 2015; Monnier and Kinnard, 2016; Anderson et al., 2018; Jones et al., 2019; Knight et al., 2019; Mayr and Hagg, 2019). The mechanisms driving transformation of the shrinking mountain glaciers into debris-covered glaciers and/or rock glaciers are still under debate (Kirkbride, 2000, 2011; Brenning, 2005; Azócar and Brenning, 2010; Gibson et al., 2017; Mayr and Hagg, 2019). The main difficulty to understand these glacier transformations is that they do not depend only on the climate variability but also on other local conditions, including lithology and topographic setting, the intensity of paraglacial readjustment and slope processes (Janke et al., 2015; Monnier and Kinnard, 2016; Anderson and Anderson, 2016; Anderson et al., 2018; Mayr and Hagg, 2019) and the amount of water supply (Kenner, 2019; Jones et al., 2019). The comprehension of the factors and processes driving these transformations is even more complicated if we consider that debris-covered glaciers and rock glaciers may react in very distinct ways and with different response times to warming, even in opposite ways, i.e. either by accelerating flow (Wirz et al., 2016; Kellerer-Pirklbauer et al., 2017; Eriksen et al., 2018; Kenner, 2019) or by slowing down and even stagnating (Emmer et al., 2015; Anderson et al., 2018; Tanarro et al., 2019; Storni et al., 2020; Ferguson and Vieli, 2020).

The Tröllaskagi Peninsula, located in central-northern Iceland, hosts over 160 glacial cirques currently occupied by debris-free glaciers, debris-covered and/or rock glaciers (Caseldine and Stotter, 1993; Lilleøren et al., 2013; Sigurðsson and Williams, 2008). These cirques have reacted differently to the intensified warming initiated at the onset of the 21st century (Fernández-Fernández et al., 2017). The cirques have very similar lithological and topoclimatic settings (altitude, precipitation and aspect), but some of them hosted debris-free glaciers. The latter may react quickly to climate changes, e.g. with advances after 5 consecutive years with summer temperature below average and winter precipitation close to average (Björnsson, 1971; Caseldine, 1985; Häberle, 1991; Kugelmann, 1991; Fernández-Fernández et al., 2017, 2019). Other cirques of this peninsula host debris-covered glaciers and rock glaciers, which have shown a delayed response to climate fluctuations, so that their front may remain stable for thousands of years (Tanarro et al., 2019; Campos et al., 2019; Fernández-Fernández et al., 2020). In addition, the pattern of glacial transformation can be even more complicated, as different sectors of one single glacier can evolve either to a debris-free glacier, a debris-covered glacier or a rock glacier, within the same cirque (Palacios et al., 2021).

Therefore, the wide variety of geomorphological settings existing in the cirques of the Tröllaskagi Peninsula makes it an excellent natural laboratory to study and improve scientific knowledge on the mechanisms behind the climate-driven transformation of mountain glaciers. Thus, the aim of this work is to study this evolution from the first stages of deglaciation, in a set of similar alpine cirques close to each other, through a multi-methodological approach. These cirques host different ice-related landforms (i.e. debris-free glaciers, debris-covered glaciers and rock glaciers) and our objectives are to contribute understanding of: (i) their origin, climatic/geomorphological significance and divergent glacial evolution; and (ii) their dynamics during the intensified warming initiated at the onset of the 21st century.

2. Study area

The cirques examined in this work are located in the Hofsdalur valley, in the Tröllaskagi Peninsula, northern Iceland (Fig. 1). The central sector of this peninsula encompasses a plateau, with elevations ranging between 1200 and 1500 m a.s.l. This plateau is constituted by Miocene basaltic flows, stacked in a regular semi-horizontal arrangement, and interspersed by sedimentary layers of a clayey nature, known as the red interbed layers (Sæmundsson et al., 1980). An intricate network of tributary valleys has been sculpted into the plateau, producing a rough terrain with relatively flat valley bottoms and near-vertical cirque walls at their headwaters. The steep slopes connecting the plateau with the valley/cirque bottoms favour slope instability. Indeed, slope failures initiated on the red interbed layers are widespread, triggering rockfalls, landslides and debris flows (Jónsson, 1976; Whalley et al., 1983; Mercier et al., 2013; Cossart et al., 2014; Decaulne et al., 2016; Sæmundsson et al., 2018).

At the Hólar meteorological station (160 m a.s.l.; Icelandic Met Office), located over 6 km from the studied cirques, the mean annual air temperature (MAAT) and annual precipitation (1961–1990 series) are 2.7 °C and 485 mm, respectively. At the town of Akureyri (40 m a.s.l.; 42 km east of the study area), MAAT was 3.4 °C and has increased by 0.95 °C in the last 30 years (Icelandic Met Office; Fernández-Fernández et al., 2017).

Mountain permafrost in Iceland is mostly found in the Tröllaskagi Peninsula. After the last deglaciation and during the Holocene Thermal Maximum (HTM), the permafrost lower limit rose from the valley floors to the Tröllaskagi summits, descending later and reaching its lowest Holocene altitude during the LIA (Lilleøren et al., 2013; Etzelmüller et al., 2020). Since the end of the LIA, the permafrost belt has risen again favouring an increase in the number of landslides (Sæmundsson et al., 2018). Modelling shows that the lower limit of permafrost in Tröllaskagi is at around ~900 m, with MAAT around −2.6 °C at most of the glacier termini (Etzelmüller et al., 2007). These values are also confirmed by 1960–2016 climate data, which show a high variability with elevation, ranging from around 600–900 m and even rising to and 1000–1150 m in windy and long-lying snow areas, and descending to around 800 m in the Hofsdalur cirques (Czekirda et al., 2019).

The Hofsdalur valley runs east to west along about 11 km until it merges into the main Hjaltadalur valley near the village of Hólar, eventually draining into Skagafjörður, the fjord at the western edge of the Tröllaskagi Peninsula (Fig. 1A, 1B). The head of the Hofsdalur valley is a cirque hosting the active Hofsjökull debris-covered glacier. To the west the adjacent cirque known as Júllogil hosts a rock glacier. The geomorphological dynamics of the debris-covered glacier and the rock glaciers of these cirques have been recently studied (Campos et al., 2019; Fernández-Fernández et al., 2020).

Aiming to complete the knowledge of the geomorphological evolution of the entire valley and to better understand the diversity of landforms and processes included therein, the four westernmost glacial cirques were selected, referred hereafter as Hofs 1–4 (Fig. 1C). The floors of these cirques are located around 780 m, and they connect with the plateau at 1070 and 1200 m, at the western and eastern sectors respectively. From east to west, the first cirque (Hofs-1) hosts a geomorphological complex including a debris-covered glacier and a rock glacier. The second cirque (Hofs-2) shows talus cones feeding a small rock glacier. The same process, but on a smaller scale, can be observed in the third cirque (Hofs-3), where the talus cones and the rock glacier are smaller than in Hofs-2. Finally, the fourth and westernmost cirque (Hofs-4), hosts only a rock glacier.

The parallel adjacent valley to the north, Hóladalur, includes a debris-covered glacier at its head, while the adjacent cirque to the

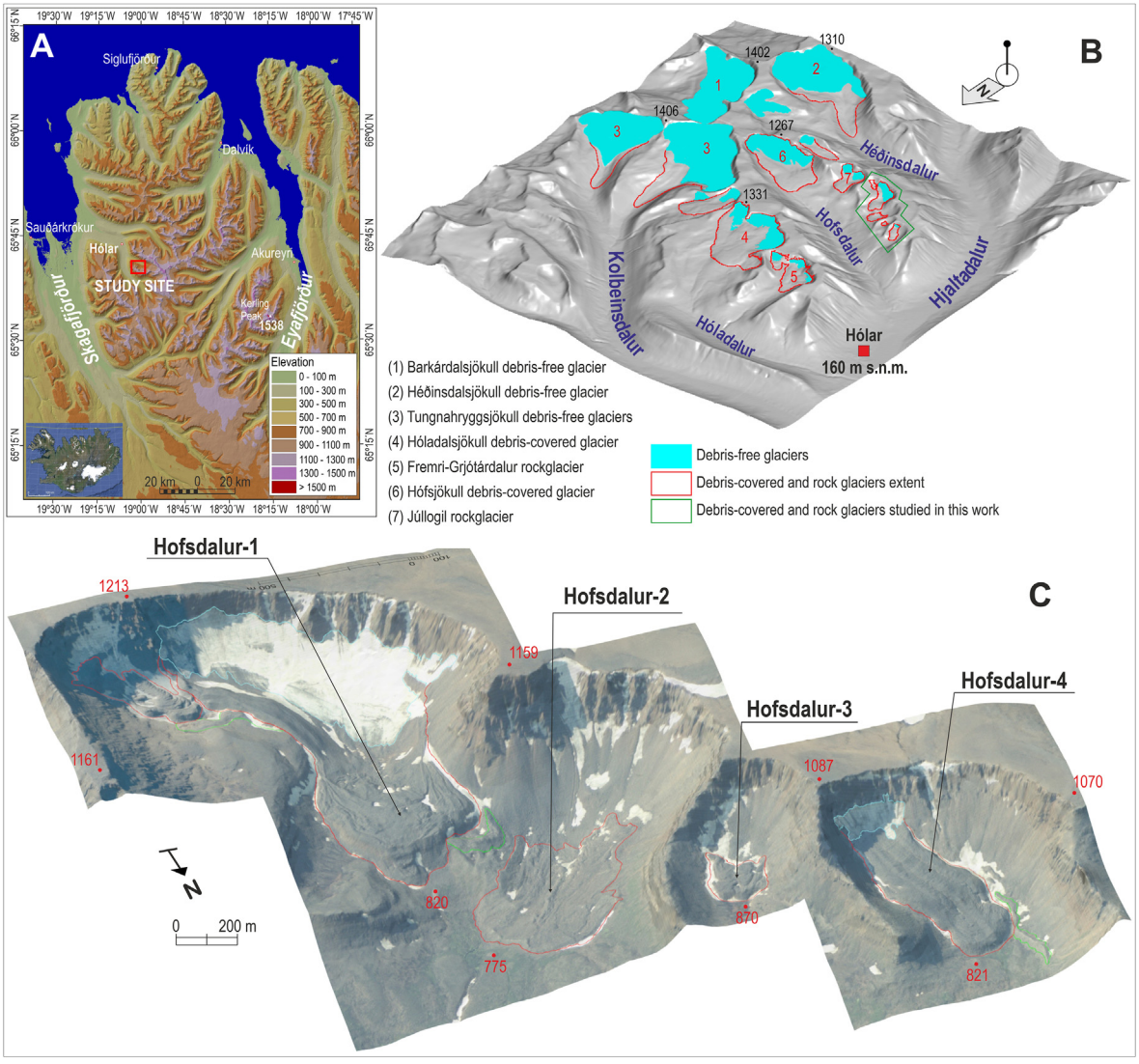

Fig. 1. Location of the study area. (A) Tröllaskagi. (B) Isometric view showing the glacial cirques in the central-western sector of Tröllaskagi. The study area is located with a green polygon. (C) Isometric view of the orthophoto of the year 2000 showing the glaciers studied in four tributary cirques of the Hofsdalur valley. (For interpretation of the references to colour in this figure legend, the reader is referred to the Web version of this article.)

west is occupied by various rock glaciers formed during different periods. The rock glaciers in both cirques have been studied according to their dynamics and origin (Kellerer-Pirklbauer et al., 2007; Tanarro et al., 2018, 2019; Fernández-Fernández et al., 2020). The adjacent valley to the south is the Héðinsdalur valley, which preserves a complex of debris-covered glacier - rock glacier - debris-free glacier at its head (Rodríguez-Mena et al., 2021; Palacios et al., 2021).

3. Methods

3.1. Geomorphological mapping

Prior to the design of the field sampling strategy, we produced a highly detailed geomorphological map, in order to identify geomorphological units and their relative chronology. For this purpose, we combined manual and automatic methods following Tanarro et al. (2019). First, a Topcon Mirror Stereoscope with 4x Binoculars was used to photo-interpret the photographic pairs from 1980, 1994 and 2019 in 3D, to draw an initial geomorphological sketch. Later, an automatic photogrammetry program (Bentley Context Capture) was used to produce stereo orthophotos (Table S1) and digital surfaces models (DSMs) from the stereo pairs of aerial photographs for each date. Both techniques permitted outlining the map geomorphological units. In a second step, the Computer-Aided Design (CAD) software Bentley MicroStation Connect was used to georeference the hand-drawn map and to vectorize the geomorphological units as polygons. The symbolization was carried out in the work interface of the desktop publishing software Corel Draw v18, following some of the most accepted standards in geomorphological mapping of mountain areas (Otto and Dikau, 2004; Lambiel et al., 2013).

3.2. ^{36}Cl CRE dating

The location of the ^{36}Cl sampling sites is shown in Table 1 and Fig. 2. During fieldwork conducted in 2018, we collected 17 samples from boulders belonging to glacial and periglacial features, in the tributary cirques of the southern slope of Hofsdalur. The targeted features were: 7 moraine boulders (HEC4-7; HEC10; HIC2-3), 7

Table 1
Geographic sample locations, topographic shielding factor, sample thickness and distance from headwall.

Sample name	Sample type	Latitude (DD)	Longitude (DD)	Elevation (m a.s.l.)	Shielding factor	Thickness (cm)	Distance from the headwall (m)
Hofsdalur-5 cirque							
HEC-4	Moraine boulder	65.6749	−19.0009	869	0.9906	3.4	1120
HEC-5	Moraine boulder	65.6748	−19.0083	868	0.9876	4.2	1170
HEC-6	Moraine boulder	65.6756	−19.0088	847	0.9854	1.8	1290
HEC-7	Moraine boulder	65.6758	−19.0089	852	0.9895	2.2	1300
Hofsdalur-4 glacier							
HEC-10	Moraine boulder	65.6795	−19.0073	775	0.9723	2.3	1870
Hofsdalur-2 cirque							
HIC-1	Erratic	65.6406	−18.8993	985	0.9797	3.5	790
HIC-2	Moraine boulder	65.6407	−18.8994	980	0.9218	3.8	690
HIC-3	Moraine boulder	65.6407	−18.8995	977	0.9218	3.5	690
Hofsdalur-5 rock glacier							
HEC-1	Rock glacier boulder (active)	65.6744	−19.0067	902	0.9932	2.8	1000
HEC-2	Rock glacier boulder (active)	65.6742	−19.0073	897	0.9925	3.8	990
HEC-3	Rock glacier boulder (active)	65.6745	−19.0066	900	0.9927	4.0	1010
Hofsdalur-4 debris-covered glacier							
HEC-8	Debris cover moraine boulder (fossil)	65.6780	−19.0091	777	0.9906	3.1	1530
HEC-9	Debris cover moraine boulder (fossil)	65.6780	−19.0091	777	0.9860	4.5	1530
Hofsdalur-2 rock glacier							
HIC-4	Rock glacier boulder (active)	65.6831	−19.0404	861	0.9817	3.1	530
HIC-5	Rock glacier boulder (active)	65.6831	−19.0404	861	0.9845	2.5	530
HIC-6	Rock glacier boulder (active)	65.6819	−19.0396	892	0.9864	4.0	400
HIC-7	Rock glacier boulder (active)	65.6819	−19.0396	892	0.9864	3.5	400

boulders from active rock glaciers (HEC1-3; HIC4-7), 2 boulders from a fossil debris-covered glacier (HEC8-9) and 1 erratic boulder (HIC-1). Pieces of the surficial layer of rock (4–1.8 cm thick) from gentle and flat-topped surfaces of the boulders were extracted by using a hammer and a chisel. The initial preparation of the samples was carried out in the "Physical Geography Laboratory" of the Universidad Complutense de Madrid, Spain, where they were crushed and sieved to the 0.25–0.8 mm fraction. The samples were subsequently chemically processed at the "Laboratoire National des Nucléides Cosmogéniques" (LN_2C) of the "Centre Européen de Recherche et d'Enseignement des Géosciences de l'Environnement" (CEREGE, Aix-en-Provence, France) following the methods described in Schimmelpfennig et al. (2011). Aliquots were taken from the bulk fraction of several representative samples from each cirque to determine the composition (major and trace elements, Table S2) to estimate the low-energy neutron flux in the samples. After an initial acid leaching to remove the atmospheric ^{36}Cl and potentially Cl-rich groundmass, 2-g aliquots were taken to determine the concentrations of the major elements (Table S3). Three chemistry blanks were prepared along with the samples (Table 2). ^{36}Cl exposure ages were calculated using the trial version of the online calculator CREp for ^{36}Cl (Martin et al., 2017; Schimmelpfennig et al., 2019, Table 2). A rock density value of 2.7 g cm^{-3} was assumed for all the samples. Correction of topographic shielding imposed by the surrounding horizon was implemented by calculating its factor with the ArcGIS toolbox designed by Li (2018) with a DEM of 0.5 m of resolution. This option was preferred to onsite horizon height measurements due to the local weather conditions at the study sites. Exposure ages were computed using the Lal/Stone time dependent scaling scheme (Lal, 1991; Stone, 2000; Balco et al., 2008), with the international standard atmosphere model (NOAA, 1976) and the atmospheric ^{10}Be-based VDM geomagnetic record (Muscheler et al., 2005; Valet et al., 2005). The following sea level-high latitude (SLHL) ^{36}Cl production rates from spallation were applied to these elements: 57.3 ± 5.2 atoms ^{36}Cl (g Ca)$^{-1}$ yr^{-1} for Ca (Licciardi et al., 2008), 148.1 ± 7.8 atoms ^{36}Cl (g K)$^{-1}$ yr^{-1} for K (Schimmelpfennig et al., 2014), 1.63 ± 0.04 atoms ^{36}Cl (g Fe)$^{-1}$ yr^{-1} for Fe (Moore and Granger, 2019), and 13 ± 3 atoms ^{36}Cl (g Ti)$^{-1}$ yr^{-1} for Ti (Fink et al., 2000). The SLHL production rate of epithermal neutrons for fast neutrons in the atmosphere at the land/atmosphere interface of 696 ± 185 neutrons (g air)$^{-1}$ yr^{-1} (Marrero et al., 2016) was applied.

Table 2 presents the ^{36}Cl CRE ages with the 1σ uncertainties. No correction for erosion or snow cover was applied, in accordance with earlier studies from Iceland. Samples were taken from blocks that protrude and are windswept, thus minimising the potential influence of snow cover. In addition, surfaces presenting signs of minimal erosion were preferred. In order to improve knowledge of the glacial evolution of Tröllaskagi, the results of the already published 12 samples included in Fernández-Fernández et al. (2020; polished surfaces and boulders from moraines, active/relict debris-covered glaciers and rock glaciers) have been recalculated with the same parameters as the new ones. The recalculated samples had been obtained in the cirques of Hóladalur and Fremri-Grjótárdalur, very close to Hofsdalur (Tables S4, S5). Table S6 includes information on displacements and elevation change of each CRE sampling site over recent decades.

3.3. Schmidt Hammer Exposure Dating (SHED)

The SHED was applied in the Hofsdalur cirques, in order to explore if weathering, and therefore the age of surface exposure of the boulders, decreased towards the headwall of the cirque in geomorphological order. Schmidt Hammer Exposure Dating (SHED) is an excellent complement of CRE dating on glacial and periglacial landforms (Matthews and Winkler, 2011; Shukla et al., 2017; Nývlt et al., 2014; Tomkins et al., 2016, 2018b; Marr et al., 2019; Wilson et al., 2019; Longhi and Guglielmin, 2020), and in dating rock glacier boulders (Kellerer-Pirklbauer et al., 2007, 2017; Rode and Kellerer-Pirklbauer, 2012; Matthews et al., 2013; Wilson and Matthews, 2016; Marr et al., 2019).

Hammer rebound readings (hereafter "R") were taken on a few CRE-sampled boulders so that the R-values can be used to extrapolate CRE ages to undated boulders belonging to the same geomorphologic units. Aiming to minimize the operator-derived error during measurement, the same person carried out the readings (Viles et al., 2011; Tomkins et al., 2016) and always used the same device (Silver Schmidt Proceq Hammer model). The operator performed 30 impacts perpendicular to the rock surface of each CRE

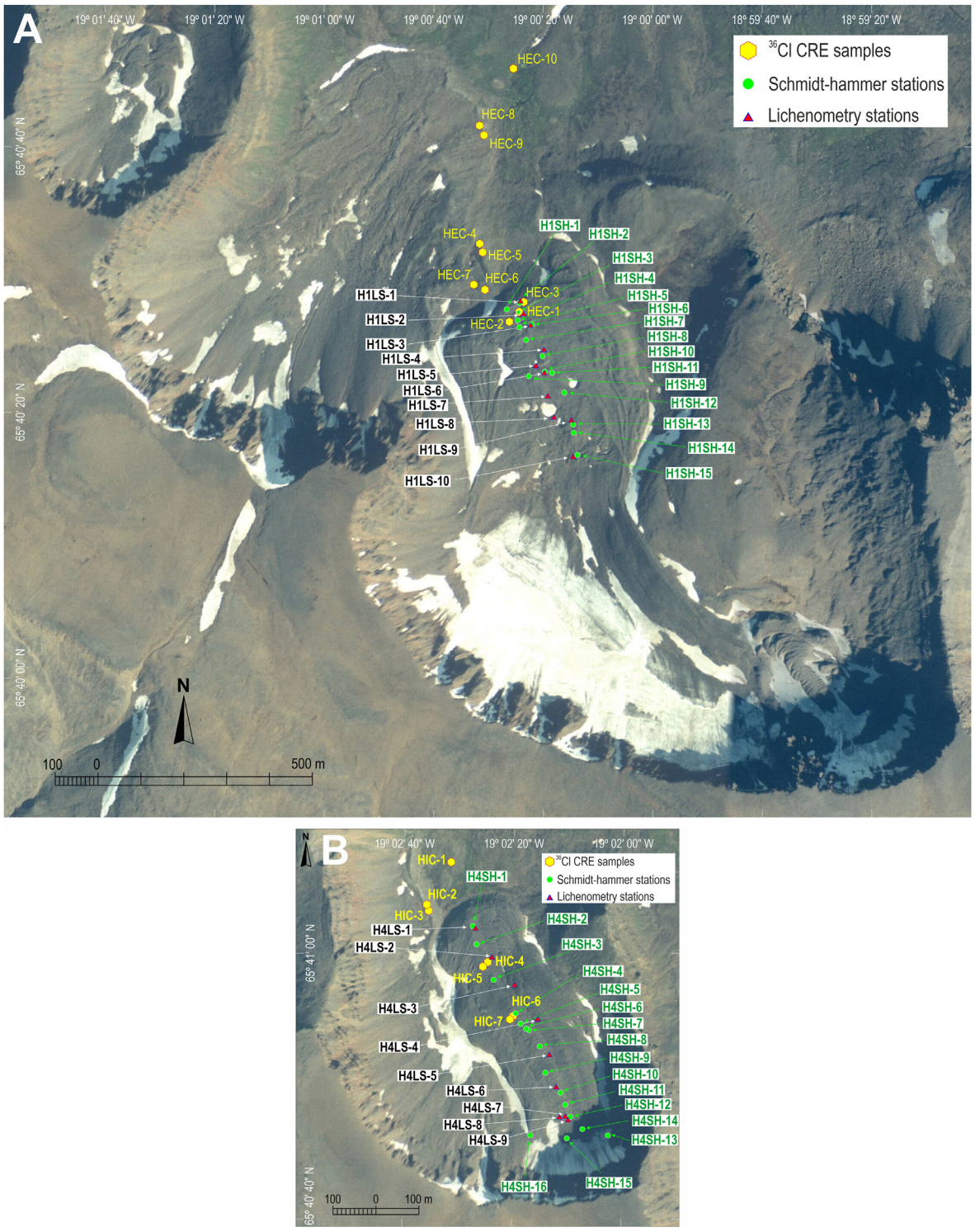

Fig. 2. Location of the sampling sites where Schmidt Hammer Exposure (SHED), Cosmic-Ray Exposure (CRE) and lichenometric (LS) dating were applied in (A) Hofs-1 cirque, and (B) Hofs-4 cirque.

sampled boulder. The largest, regular and not heavily lichen-covered boulders were preferred (Aydin, 2009; Matthews and Owen, 2010; Viles et al., 2011). The measurements were taken in a dry period to avoid the alteration of the R values due to moisture in the rock (Sumner and Nel, 2002; Viles et al., 2011). The hammer was periodically calibrated using the manufacturer's test (Wilson et al., 2019). For each sampling site, we obtained the arithmetic mean, standard deviation, standard error, and 95% confidence interval (Niedzielski et al., 2009; Tomkins et al., 2016, 2018a and 2018b; Wilson et al., 2019). Measurements were performed along longitudinal transects over debris-covered sectors of a glacier (Hofs-1) and a rock glacier (Hofs-4), from their front to the boulders close to the cirque wall. Significant scatter in the measurement was not expected as all the sampled boulders belonged to the same

Table 2
^{36}Cl CRE dating results. The ^{35}Cl spike was manufactured in-house (ID: 261,018, 6.019 ± 0.115 mg Cl g^{-1},^{35}Cl/^{37}Cl ratio 296.9 ± 3.6. AMS measurements were conducted at the ASTER facility of CEREGE and normalized to the in-house standard SM-CL-12 with an assigned ^{36}Cl/^{35}Cl ratio value of (1.428 ± 0.021) x 10^{-12} (Merchel et al., 2011) and assuming a natural ^{35}Cl/^{37}Cl ratio of 3.127. The numbers in italics correspond to the analytical uncertainty at one standard level.

Sample name	Sample weight (g)	Mass of Cl in spike (mg)	^{35}Cl/^{37}Cl	^{36}Cl/^{35}Cl (10^{-14})	[Cl] in sample (ppm)	[^{36}Cl] (10^4 atoms g^{-1})	^{36}Cl CRE age (ka)
Hofsdalur-5 cirque							
HEC-4	42.82	1.824	11.755 ± 0.226	12.137 ± 0.712	19.5 ± 2.3	11.921 ± 0.789	7.67 ± 0.78 (*0.51*)
HEC-5	42.44	1.820	11.408 ± 0.229	9.994 ± 0.626	20.5 ± 2.4	9.984 ± 0.701	7.78 ± 0.83 (*0.56*)
HEC-6	41.8	1.812	8.020 ± 0.205	15.000 ± 0.860	35.6 ± 4.3	18.051 ± 1.335	12.37 ± 1.29 (*0.93*)
HEC-7	43.12	1.823	19.694 ± 0.594	18.505 ± 1.010	9.7 ± 1.2	15.746 ± 0.907	11.56 ± 1.13 (*0.68*)
Hofsdalur-4 glacier							
HEC-10	42.85	1.815	7.751 ± 0.178	14.237 ± 0.899	36.9 ± 4.5	17.126 ± 1.358	12.48 ± 1.36 (*1.01*)
Hofsdalur-2 cirque							
HIC-1	41.12	1.821	23.267 ± 0.442	16.818 ± 1.008	8.2 ± 1.0	14.564 ± 0.901	8.98 ± 0.91 (*0.56*)
HIC-2	42.26	1.823	9.468 ± 0.496	12.124 ± 0.801	27.2 ± 3.8	13.215 ± 1.058	8.23 ± 0.91 (*0.67*)
HIC-3	42.58	1.820	7.358 ± 0.180	13.872 ± 0.829	40.8 ± 5.0	17.463 ± 1.373	10.4 ± 1.15 (*0.83*)
Hofsdalur-5 rock glacier							
HEC-1	85.82	1.811	8.185 ± 0.163	3.828 ± 0.343	16.6 ± 2.0	2.198 ± 0.222	1.58 ± 0.20 (*0.16*)
HEC-2	87.78	1.804	5.768 ± 0.197	5.218 ± 1.009	31.5 ± 4.3	3.956 ± 0.822	2.39 ± 0.54 (*0.51*)
HEC-3	86.96	1.801	6.558 ± 0.273	4.001 ± 0.380	24.3 ± 3.4	2.669 ± 0.310	1.57 ± 0.22 (*0.19*)
Hofsdalur-4 debris-covered glacier							
HEC-8	86.64	1.813	5.578 ± 0.115	17.186 ± 1.065	34.7 ± 4.3	13.877 ± 1.281	9.58 ± 1.16 (*0.90*)
HEC-9	85.34	1.811	6.993 ± 0.154	22.762 ± 1.136	22.1 ± 2.7	14.815 ± 1.077	10.88 ± 1.14 (*0.80*)
Hofsdalur-2 rock glacier							
HIC-4	86.75	1.811	4.749 ± 0.080	5.380 ± 0.540	52.5 ± 6.5	5.560 ± 0.650	3.20 ± 0.46 (*0.39*)
HIC-5	88.57	1.815	6.078 ± 0.129	6.720 ± 1.116	28.1 ± 3.4	4.796 ± 0.854	2.88 ± 0.57 (*0.52*)
HIC-6	87.5	1.804	6.208 ± 0.136	5.649 ± 0.482	27.0 ± 3.3	3.965 ± 0.418	2.40 ± 0.32 (*0.26*)
HIC-7	90.11	1.806	8.494 ± 0.155	7.596 ± 0.527	14.9 ± 1.8	4.070 ± 0.332	2.59 ± 0.29 (*0.21*)
Blanks[a]					***Total atoms Cl*** (10^{17})	***Total atoms ^{36}Cl*** (10^4)	
BK-2		1.821	202.688 ± 6.266	0.056 ± 0.029	2.051 ± 0.306	1.776 ± 0.891	
BK-3		1.805	153.865 ± 3.733	0.058 ± 0.022	4.086 ± 0.507	1.823 ± 0.692	

BK-2 was processed with samples HEC-4, HEC-5, HEC-6, HEC-7, HEC-10, HIC-1, HIC-2, and HIC-3; BK-3 was processed with samples HEC-1, HEC-2, HEC-3, HEC-8, HEC-9, HIC-5. HIC-6, and HIC-7.

lithology, geological formation (Tertiary Basalts Formation) and environmental conditions for weathering (i.e., climate). The results are shown in Tables S7 and S8, including data on the stability of each sampling site over recent decades.

3.4. Lichenometric dating

A number of lichen stations were established along transects crossing a number of main ridges of the rock glaciers, aiming to obtain a minimum age estimate. This technique was applied on those landforms expected to be very young (last few centuries?/ 20th century?) and thus below the lower limit of the CRE dating applicability. Special care was taken when choosing their locations so that the lichen growth was not influenced by local topo-climatic constraints (i.e., snowpack duration). In each lichenometry station, the largest *Rhizocarpon geographicum* and *Porpidia* cf. *soredizodes* thalli were searched within a 10-m buffer, preferring those with circular- or ellipsoidal-shapes, non-coalescent and located on smooth horizontal boulder surfaces. Measurements were taken in accordance with the method proposed by Fernández-Fernández et al. (2019).

The lichen-derived age calculations from the *Rhizocarpon geographicum* thalli were done by applying the 0.44 mm yr^{-1} growth rate obtained by Kugelmann (1991) for Svarfaðardalur-Skíðadalur, as to the date, it relies on the highest number of control points (surfaces of known age) so far in the Tröllaskagi Peninsula. For the *Porpidia* cf. *soredizodes* specimens, the growth rate of 0.737 mm yr^{-1} estimated by Fernández-Fernández et al. (2019) was applied. We assumed a 20-yr colonization lag for the *Rhizocarpon geographicum* thalli and 10-yr for *Porpidia soredizodes* thalli, as observed in the neighbouring Vesturdalur and Austurdalur valleys (Fernández-Fernández et al., 2019), some 7 km away. Where thalli coalescence was prevailing, no lichen was measured in any of the stations. In Iceland this usually occurs on stable surfaces exposed for more than 160–220 years, according to the literature (see Maizels and Dugmore, 1985; Thompson and Jones, 1986; Evans et al., 1999). The results are shown in Tables 3 and 4, including information on the stability (vertical and horizontal movement) of each station over the last decades.

3.5. Boulder displacement

The mobility of the rock glaciers and debris-covered sectors of glaciers has been studied through conventional photogrammetric techniques applied to historical aerial photographs (1980, 1994 and 2019). Those for the first two years were obtained from the National Land Survey of Iceland and those of 2019 photos were obtained from "Loftmyndir ehf" company. The historical photographs of 1980 and 1994 were scanned at a high resolution, 20 and 15 μm, respectively (Janke, 2005; Tanarro et al., 2019)). Then we restituted the most visible blocks on the glacier surface at every available date, through a digital photogrammetric work station (DPWS) Digi3D.NET. The restitution procedure was as follows:

First, we corrected the stereo pairs geometrically to: (i) obtain stereoscopic models of each flight, after adjusting the internal orientation of the stereo pairs according to the calibration parameters of the cameras used; and (ii) correct the absolute orientation to obtain the X, Y and Z terrain coordinates. For this purpose, stable control points were extracted from the Digital Elevation Model (DEM) and the orthophoto from the year 2000. The resulting absolute orientation gave a relatively small root mean square error (RMSE) for all flights, of less than 0.4 m (Table S1).

In a second step 3D digital stereo plotting, through the DPWS Digi3D.NET, permitted recording of X, Y and Z coordinates of the common blocks identified at each date (1980, 1994 and 2019). All sampled boulders (CRE, SHED and lichenometry) were also accounted in the mobility monitoring. The centroid of each block was considered as a single point. The coordinates of each point

Table 3
Surface exposure ages at Hofs-1, estimated from 0.44 mm yr to 1 lichen growth rate for *Rhizocarpon geographicum* (RG) (Kugelmann, 1991) and 0.737 mm yr^{-1} for *Porpidia soredizodes* (PS) (Fernández-Fernández et al., 2019) assuming growth rate and a 10, 15 and 20-year colonization lag. following. The considered colonization ages for *Rhizocarpon geographicum* is 20 years and for *Porpidia soredizodes* is 10 years (Fernández-Fernández et al., 2019) and these ages are outstanding in the table and in the text. Also, the table includes information on the stability (horizontal movement and change elevation) of each lichen station over the last decades.

Lichen Station	*(RG)* Minimum circle diameter (mm)	(PS) Minimum circle diameter (mm)	CE Age according to RG	CE Age according to PS	Location	Coordinates (LAMCC. WGS84)	Distance from headwall (m)	Altitude (m a.s.l.) 1980	Altitude (m a.s.l.) 1994	Altitude (m a.s.l.) 2019	1994–1980 Average Velocity (m/year)	2019–1994 Average Velocity (m/year)	1994–1980 Elevation Changes (m)	2019–1994 Elevation Changes Mean (m)
H1LS-1	Coalescing thalli	Coalescing thalli	**>1820**	**>1820**	Frontal ridge	65° 40′ 28.3306″ N, 19° 00′ 23.9872″ W	1046.58	903.729	903.965	902.154	0.140	0.206	−0.451	−3.342
H1LS-2	Coalescing thalli	Coalescing thalli	**>1820**	**>1820**	Second ridge -Third ridge	65° 40′ 27.4186″ N, 19° 00′ 23.4305″ W	1008.65	908.038	906.947	905.589	0.136	0.160	−0.326	−2.265
H1LS-3	Coalescing thalli	Coalescing thalli	**>1820**	**>1820**	Fourth ridge	65° 40′ 26.5860″ N, 19° 00′ 21.5357″ W	979.27	915.231	914.827	911.967	0.135	0.167	−0.779	−3.244
H1LS-4	Coalescing thalli	Coalescing thalli	**>1820**	**>1820**	Fifth ridge - Hummoky feature	65° 40′ 25.0473″ N, 19° 00′ 20.0087″ W	921.60	918.196	918.169	915.205	0.106	0.129	−0.533	−3.436
H1LS-5	Coalescing thalli	Coalescing thalli	**>1820**	**>1820**	Younger push moraine	65° 40′ 23.4738″ N, 19° 00′ 20.7566″ W	886.44	921.555	921.348	919.294	0.092	0.105	−0.242	−3.155
H1LS-6	41.1	179.7	**1904**	**1764**	Younger push moraine	65° 40′ 22.5234″ N, 19° 00′ 19.7328″ W	867.42	925.323	924.559	921.616	0.087	0.076	−0.564	−3.475
H1LS-7	28.8	105.1	**1932**	**1865**	Ridges into the depression	65° 40′ 20.8397″ N, 19° 00′ 19.4706″ W	815.08	922.571	921.807	918.869	No interpolated	0.090	No interpolated	−3.119
H1LS-8	34.2	122.0	**1920**	**1842**	Ridges into the depression	65° 40′ 19.0367″ N, 19° 00′ 17.4940″ W	746.61	915.427	917.072	911.853	No interpolated	0.142	No interpolated	−4.858
H1LS-9	56.3	95.4	**1870**	**1878**	Ridges into the depression	65° 40′ 19.3226″ N, 19° 00′ 14.6516″ W	760.00	925.274	924.838	921.779	No interpolated	0.135	No interpolated	−3.473
H1LS-10	16.0	40.5	**1962**	**1953**	Ridges into the depression	65° 40′ 16.8289″ N, 19° 00′ 14.2168″ W	674.25	915.837	915.81	913.325	No interpolated	0.272	No interpolated	−3.155

Table 4
Surface exposure ages at Hofs-4, estimated from 0.44 mm yr^{-1} lichen growth rate for *Rhizocarpon geographicum* (RG) (Kugelmann, 1991) and 0.737 mm yr^{-1} for *Porpidia soredizodes* (PS) (Fernández-Fernández et al., 2019) assuming growth rate and a 10, 15 and 20-year colonization lag, following. The considered colonization ages for *Rhizocarpon geographicum* is 20 years and for *Porpidia soredizodes* is 10 years (Fernández-Fernández et al., 2019) and these ages are outstanding in the table and in the text. Also, the table includes information on the stability (horizontal movement and change elevation) of each lichen station over the last decades.

Lichen Station	*(RG)* Minimum circle diameter (mm)	(PS) Minimum circle diameter (mm)	CE Age according to RG	CE Age according to PS	Location	Coordinates (LAMCC. WGS84)	Distance from headwall (m)	Altitude (m a.s.l.) 1980	Altitude (m a.s.l.) 1994	Altitude (m a.s.l.) 2019	1994–1980 Average Velocity (m/year	2019–1994 Average Velocity (m/year	1994–1980 Elevation Changes (m)	2019–1994 Elevation Changes Mean (m)
H4LS-1	Coalescing thalli	Coalescing thalli	**>1820**	**>1820**	Frontal ridges	65° 41′ 02.1004″ N, 19° 02′ 26.4067″ W	691.86	850.247	850.209	848.342	0.184	0.150	−0.702	−2.657
H4LS-2	Coalescing thalli	Coalescing thalli	**>1820**	**>1820**	Second ridges - Third ridges	65° 40′ 59.8308″ N, 19° 02′ 23.2864″ W	613.63	866.353	866.331	863.276	0.177	0.154	−0.704	−1.507
H4LS-3	Coalescing thalli	Coalescing thalli	**>1820**	**>1820**	Third ridges - Fourth ridges	65° 40′ 57.6398″ N, 19° 02′ 18.7496″ W	533.48	900.97	900.426	895.791	0.158	0.206	−0.533	−4.283
H4LS-4	Coalescing thalli	Coalescing thalli	**>1820**	**>1820**	Fourth ridges	65° 40′ 55.1049″ N, 19° 02′ 15.1011″ W	440.15	917.18	917.498	915.904	0.154	0.144	−0.448	−1.545
H4LS-5	37.4	104.5	**1914**	**1866**	Fourth ridges - Fifth ridges	65° 40′ 52.0373″ N, 19° 02′ 12.7472″ W	352.23	928.825	928.459	926.769	0.165	0.131	−0.355	−2.060
H4LS-6	37.2	121.1	**1913**	**1844**	Fifth ridges - Younger push moraine	65° 40′ 49.7978″ N, 19° 02′ 11.9764″ W	276.94	936.313	936.208	934.383	0.162	0.109	0.048	−2.400
H4LS-7	28.7	48.0	**1932**	**1942**	Ridges into the depression	65° 40′ 47.7985″ N, 19° 02′ 09.7768″ W	208.00	937.672	938.453	936.426	Cover by snow	Cover by snow	Cover by snow	Cover by snow
H4LS-8	14.5	8.2	**1965**	**1997**	Ridges into the depression	65° 40′ 47.7521″ N, 19° 02′ 11.1909″ W	210.95	938.213	938.764	936.622	Cover by snow	Cover by snow	Cover by snow	Cover by snow
H4LS-9	No present	4.24	**<1999**	**2002**	Ridges into the depression	65° 40′ 47.6321″ N, 19° 02′ 09.3976″ W	194.21	938.03	940.075	936.769	Cover by snow	Cover by snow	Cover by snow	Cover by snow

(boulder) in the different dates were integrated in a database. Finally, these data were processed in the Geographic Information System (GIS) ArcMap 10.8, to obtain the displacement vector and to derive the speed of each block and the elevation change between dates. An interpolation tool (a 'kriging' routine) was used to map the spatial pattern of surface boulder displacement and elevation changes of the studied rock glaciers and debris-covered glaciers.

In order to show mobility around each sampling site (CRE, SHED or lichens), the statistics of both the horizontal displacement and the elevation changes within a buffer of 5 m were obtained. The results are shown in Tables 3 and 4 and Tables S6, S7, S8 and the number of identified boulders is summarized for the different dates in Tables S9 and S10.

3.6. Quantification of recent glacier changes, glacier reconstruction and equilibrium line altitude (ELA) calculations

The glacier of Hofs-1 cirque, the largest and most complex one, has been selected as the main focus of this study, to obtain a better understanding of the transformations that it has undergone during its recent evolution. The following steps were applied:

(i) *Elaboration of high-resolution DSM.* Structure from Motion photogrammetry (SfM) has been applied to aerial photographs to produce a high-resolution DSM and orthophotos (Westoby et al., 2012; Mertes et al., 2017). This technique has proven to be suitable for monitoring the recent evolution of glaciers (Piermattei et al., 2015, 2016; Mölg and Bolch, 2017; Mertes et al., 2017; Vargo et al., 2017; Midgley and Tonkin, 2017). In this work SfM has been applied through the Bentley Context-Capture photogrammetry software to generate georeferenced 3D meshes from the 1980, 1994 and 2019 aerial photographs. Control points (X, Y, Z coordinates), have been established by traditional photogrammetry, using the DPWS Digi3D.NET to later georeference the models in the 3D photo-reconstruction processes. With a calculated global 3D RMSE, the uncertainty was lower than 1.76 m (Table S11).

(ii) *Recent glacier surface changes.* From the high-resolution DSMs we obtained a DEM of difference, later used to quantify changes in glacier thickness (Piermattei et al., 2016; Mölg and Bolch, 2017; Ewertowski et al., 2019). These were obtained in a GIS environment through the Geomorphic Change Detection software (https://gcd.riverscapes.xyz/), calculating the total volume of surface lowering or raising (Table 5), as well as the average thickness difference. These analyses were carried out in two reference polygons, i.e. for the debris-free and the debris-covered sectors.

(iii) *Glacier reconstruction.* 2D and 3D glacier reconstruction for the most extensive glacial stages, was carried out in the GIS environment of ArcGIS 10.3. For the most recent stages (from 1980 onwards) orthophotos and DSMs elaborated with SfM were used to map the surface extent and obtain the former topography of the Hofs-1 glacier at each date. For the same purpose, the 2000 DEM and orthophoto from "Loftmyndir ehf" were also used. Glacier geometry was reconstructed from geomorphological evidence for the oldest stages. As the current deglaciated area consists of a chaotic and unconsolidated accumulation of rocks formerly constituting a debris-covered glacier, it prevents using rheological models to produce former glacier equilibrium profiles (Van der Veen, 1999) and application of numerical-based reconstructions (e.g. Pellitero et al., 2016). Thus, the hand drawing "cartographical approach" was chosen as a suitable alternative (Sissons, 1974; Ballantyne, 1989; Dahl and Nesje, 1992; Pellitero et al., 2015). Former glacier contours were drawn manually so that they resemble the topography typically observed in current glaciers realistically, i.e., increasing contour concavity towards the headwall (accumulation area) and increasing convexity to the terminus (ablation area). To further ease glacier reconstructions in the oldest stages, the same upper rim from 1980 was assumed (Koblet et al., 2010).

(iv) *Measurements of past glacier volume, length and area.* Glacier length and area over the two stages was obtained in ArcGIS 10.3: the former was obtained by measuring a centreline connecting the points with the highest and lowest elevations at the glacier edges and the latter from the "Calculate Geometry" function. Finally, ice volumes were estimated through an "area volume scaling" (Bahr et al., 1997; 2015). For more details on the application of this method in Tröllaskagi cirque glaciers, the reader is referred to Fernández-Fernández and Andrés (2018). The results are shown in Table 6.

(v) *Equilibrium-line altitude (ELA) calculations.* ELAs of the different stages were calculated by using the automatic ArcGIS toolbox "ELA calculation" (Pellitero et al., 2015), where the DEM of the glacier surface was input. We assumed that the glacier had a similar size just before its transformation into a debris-covered glacier or rock glacier and

Table 5
Surface lowering in Hosf-1 cirque from 1980 to 2019. Note that the cirque in 1994 photo has a deep snow cover, which alters the data in this year.

Debris-free sector of the glacier and intermediate depression.	**1980–2019**	**1980–1994**	**1994–2019**
Estimate total area of surface lowering (ha)	23.18	0.95	23.16
Estimate total area of surface raising (ha)	2.65×10^{-3}	12.53	6×10^{-4}
Estimate total area of volume surface lowering (hm^3)	4.71 ± 0.41	0.0242 ± 0.0103	5.076 ± 0.41
Estimate total area of volume raising (hm^3)	5.325^{e-5} ±4.7^{e-5}	0.36 ± 0.14	1.2^{e-5} ± 1.1^{e-5}
Average depth of surface lowering (m)	20.31 ± 1.76	2.55 ± 1.09	21.92 ± 1.76
Average depth of Surface raising (m)	2.01 ± 1.76	2.85 ± 1.09	2.0 ± 1.76
Percent Elevation Lowering	100%	6%	100%
Percent Surface Raising	0%	94%	0%
Debris-covered sector of the glacier	**1980–2019**	**1980–1994**	**1994–2019**
Estimate total area of surface lowering (ha)	36.49	22.83	27.36
Estimate total area of surface raising (ha)	1.01	5.7	5.62
Estimate total area of volume surface lowering (hm^3)	1.73 ± 0.64	0.58 ± 0.25	1.35 ± 0.48
Estimate total area of volume raising (hm^3)	0.032 ± 0.018	0.144 ± 0.062	0.15 ± 0.099
Average depth of surface lowering (m)	4.74 ± 1.76	2.55 ± 1.09	4.93 ± 1.76
Average depth of Surface raising (m)	3.15 ± 1.76	2.52 ± 1.09	2.66 ± 1.76
Percent Elevation Lowering	98%	80%	90%
Percent Surface Raising	2%	20%	10%

according to this criterion, we calculated the ELAs for this phase. We applied the AAR (Accumulation Area Ratio; Meier and Post, 1962; Porter, 1975) and AABR (Area Altitude Balance Ratio; Osmaston, 2005) methods, implementing the ratios 0.67 (Stötter, 1990; Caseldine and Stotter, 1993) and 1.5 ± 0.4 (Fernández-Fernández et al., 2017, 2018, 2019), respectively. The results are shown in Table 6.

4. Results

4.1. Geomorphological survey

4.1.1. Cirque Hofs-1

From east to west: the first cirque (Hofs-1) hosts a >1 km-long glacier, with its head at 1040–1100 m altitude and its front at 860–880 m. This cirque has six differentiated geomorphological units (Fig. 3A and B, Fig. S1, S2):

(Unit i) The upper part of the glacier constitutes a *debris-free sector* (~400 m long) starting from the headwall of the cirque.

(Unit ii) The lower frontal sector is *debris-covered* (300 m long and 600 m wide), with abundant longitudinal and transverse ridges. The thin debris mantle (~1 m thick) favours the development of several collapse depressions resulting from the melting of the underlying ice.

(Unit iii) *A large intermediate depression* (300 m long and 50 m deep), located between the debris-free and the debris-covered sectors, with several collapse depressions and lakes occupying the bottom of this unit. A number of landforms were identified in this sector:

(a) *Relatively young frontal push moraines*, at the northern edge between the depression and the debris-covered glacier. These must have been deposited by the debris-free glacier advancing and overlapping the debris-covered area, to later melt and leave the intermediate depression.
(b) *Flow and creep lobate landforms* formed on the slopes surrounding the intermediate depression. Most of these features show flow in the opposite direction to the glacier, favoured by the steep slopes of the depression.

(Unit iv) *Incipient rock glacier*, only 100 m long, located in front of the debris-covered area.

(Unit v) *Old push moraine ridges*, which are clearly visible to the northwest and east sides of the debris-covered sector and are older than the push moraine in unit iii.

(Unit vi) *Small rock glacier*, located at the easternmost rim of this cirque. It is ~300 m long and its surface displays numerous transverse ridges. Some collapse features show evidence of the existence of interstitial ice within the debris accumulation.

The surface morphology of the debris-covered glacier Hofs-1 showed significant changes throughout the stereo-orthophotos from 1980, 1994 and 2019 (Figs. S3, S4, S5) and the orthophoto from 2000. The main changes are related to (i) the retreat of the debris-free sector of the glacier, which has left several ridges; and (ii) the erosion of the older push moraine ridge (unit v) in front of the debris-covered sector of the glacier (Fig. 4). Postglacial erosion processes have carved a channel on the outer flank of the central sector of the moraine, and the associated sediments are deposited in an alluvial fan at the glacier foreland.

4.1.2. Cirque Hofs-2

The adjacent cirque to the west, Hofs-2, hosts a large debris mantle (600 m long) starting at 830–840 m altitude and with its front at 770–780 m. Associated landforms are related to a hummocky moraine type (Fig. 3), with widespread longitudinal ridges separated by furrows. Bedrock was observed at the bottom of the collapsed depressions and in sections cut into the debris, suggesting that the landform is ice free at present. Consequently, we define it as a *collapsed debris-covered glacier*. In the glacier foreland, there are several *erratic boulders* that reveal the receding stage of a glacier that was probably debris-free. In the upper part of the cirque floor, at the foot of the wall, there is relatively young *small push moraine* enclosing a depression (Fig. 3).

4.1.3. Cirque Hofs-3

To the west, the cirque Hofs-3 includes a small *rock glacier* (150 m long) located between 900 m and 870 m altitude, above an old push moraine.

4.1.4. Cirque Hofs-4

The westernmost cirque, Hofs-4, hosts a *rock glacier* (540 m long) located from 930 to 940 m altitude at its head to 820 m at its front. This rock glacier displays transverse surface ridges, arranged as arches convex down-valley. Some collapse depressions expose interstitial ice. A small debris-free glacier is located above the rock glacier. The two features are separated by an *intermediate depression* with similar characteristics to that described in the Hofs-1 cirque. At the northern edge of the depression, *young push moraines* overlapping the rock glacier can be observed (Figs. 2, 5 and 6). At the same time, the northwestern sector of the rock glacier overlaps an *old lateral moraine*. Several scattered erratic boulders (up to 4 m long) are distributed in front of the rock glacier.

4.2. ^{36}Cl CRE dating

The spatial distribution of the sampled landforms is shown in Table 2, Table S6 and Figs. 2 and 5–8.

In Hofs-1 cirque, we sampled the old push moraines partially overlapped by the front of the debris-covered glacier (Table 2, Table S6 and Figs. 2, 5 and 6). At the northwest part of the cirque, four old push moraine ridges were identified, although their limited size and spatial arrangement impeded reconstructing the former glacier geometry. We took two samples from boulders of the inner ridge moraine (HEC-4 and 5) and two more from the outer ridge (HEC-6 and 7). The samples of each ridge yielded consistent ages: 7.7 ± 0.5 and 7.8 ± 0.6 ka in the inner ridge, (average age: 7.7 ± 0.5 ka); and 12.4 ± 0.9 and 11.6 ± 0.7 ka in the outer ridge (average age: 12.0 ± 0.8 ka). Three boulders (HEC-1, 2 and 3) from the stable outermost ridge of the debris-covered sector of the glacier yielded much younger ages than those of the old push moraines: 1.6 ± 0.2, 2.4 ± 0.5 and 1.6 ± 0.2 respectively (average: 1.8 ± 0.3 ka).

In the Hofs-2 cirque (Table 2, Table S6 and Figs. 2, 5 and 7), one sample from one of the most prominent erratic boulders (HEC-10) gave an age of 12.5 ± 1.0 ka, and samples from two boulders from the most advanced, stable ridges of the collapsed debris-covered glacier (HEC-8 and HEC-9) returned ages of 9.6 ± 0.9 ka and 10.9 ± 0.8 ka, respectively (average: 10.2 ± 0.8 ka).

Finally, in the Hofs-4 cirque (Table 2, Table S6 and Figs. 2, 5 and 8), one sample from the biggest erratic boulder (HIC-1), farthest from the wall, and two boulders (HIC-2 and HIC-3) from the lateral moraine yielded 9.0 ± 0.6 ka, 8.2 ± 0.7 ka and 10.4 ± 0.8 ka, respectively (average: 9.2 ± 0.7 ka). Four boulders (HIC-4, HIC-5, HIC-6 and HIC-7) from stable positions on the transverse ridges of the intermediate rock glacier sectors yielded 3.2 ± 0.4 ka, 2.9 ± 0.5 ka, 2.4 ± 0.3 ka and 2.6 ± 0.2 ka, respectively (average: 2.8 ± 0.4 ka).

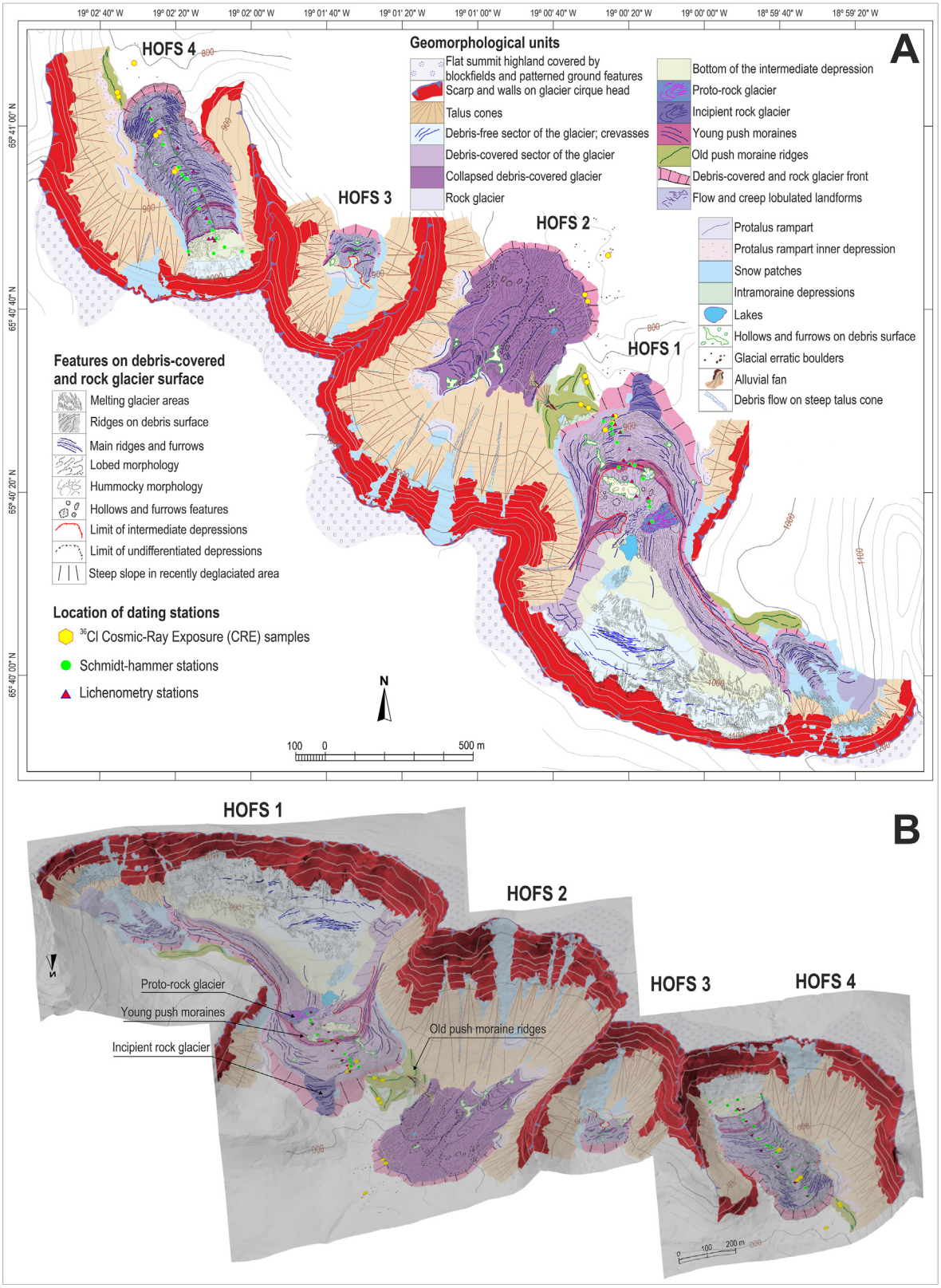

Fig. 3. (A) Geomorphological map of the Hofsdalur tributary cirques. (B) Three dimensional isometric view.

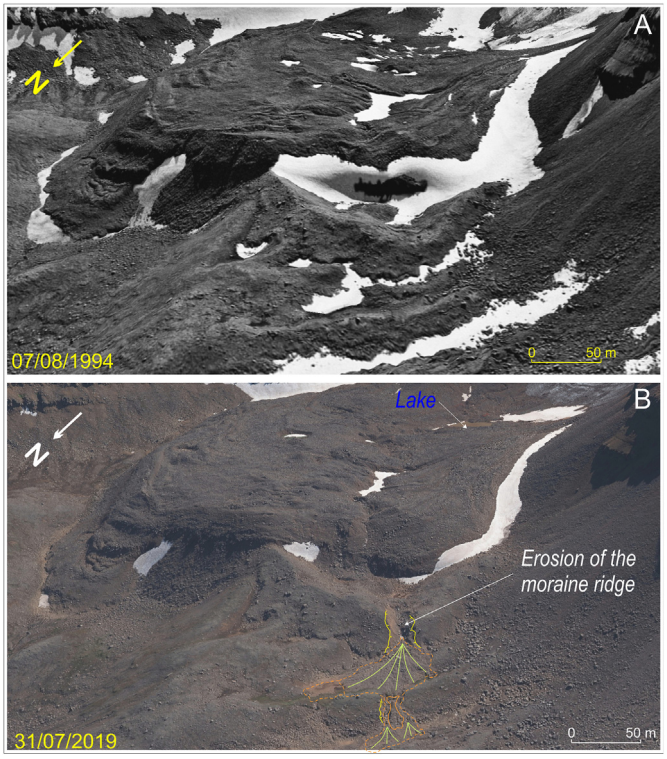

Fig. 4. Oblique comparison of the front of the debris-covered glacier at Hofs-1, on the 1994 and 2019 orthophotos. Note the recent erosion of the morainic ridge and the alluvial fan formation.

4.3. SHED

The SHED was applied in the Hofs-1 cirque, in 15 sites from the front of the debris-covered sector to the intermediate depression (Table S7 and Figs. 2, 5 and 6). In the debris-covered area (sampling sites H1SH-1 to H1SH-7) there is no clear tendency and R-values showed a random distribution ranging from 48.1 to 57.5 (mean 52.0 ± 1.0, n = 7). The measurements on the younger push moraine yielded similar R-values as in the debris-covered glacier sector (sites H1SH-9 to H1SH-12), from 46.1 to 54.1 (50.0 ± 0.9, n = 3). In the intermediate depression, boulders (sites H1SH-13 to H1SH-15) yielded higher R-values from 65.2 to 72.2 (68.4 ± 0.8, n = 3), revealing less weathered and much younger surfaces.

Another SHED transect was carried out in the Hofs-4 cirque along the rock glacier, from its front to the interior of the intermediate depression, with 16 measuring sites (Table S8 and Figs. 2, 5 and 8). In this case, the R-values in the debris-covered area (sites H4SH-1 to H4SH-7) showed a broader range, from 37.9 to 59.6 (49.1 ± 1.1, n = 9) following a random arrangement. Two sites in the younger push moraines (H4SH-10 and H4SH-11) showed scattered R-values, with 62.9 and 45.7 (54.3 ± 0.9, n = 2). Finally, unlike in the Hofs-1 cirque, the four sites in the intermediate depression (sites H4SH-12, H4SH-13, H4SH-15 and H4SH-16) did not yield much higher values, ranging from 49.0 to 62.6 (54.4 ± 1.1, n = 4).

4.4. Lichenometric dating

The results obtained at the lichen stations of the cirque Hofs-1 are summarized in Table 3 and Figs. 2, 5 and 6. The first five stations (H1LS-1 to 5), on the debris-covered sector of the glacier showed lichen coalescence, which means that the surface has been exposed for more than 160–220 years (see Maizels and Dugmore, 1985; Thompson and Jones, 1986; Evans et al., 1999). Lichen measurements of the stations at the push moraines, between the debris-covered sector and the depression (H1LS-6 to H1LS-9), yielded a range of minimum dates between 1904 and 1923 CE according to *Rhizocarpon geographicum* thalli, but did not follow a consistent chronological sequence. *Porpidia* cf. *soredizodes* thalli provided a logical chronological order ranging between 1764 and 1870 CE, with younger ages towards the cirque head. At the lichen station located next to the depression (H1LS-10), in front of the debris-free glacier, ages varied between 1965 CE (*Rhizocarpon geographicum)* and 1956 CE (*Porpidia soredizodes).*

At the cirque Hofs-4 (Table 4 and Figs. 2, 5 and 8), on the surface of the rock glacier (stations: H4LS-1 to H4LS-4), lichen coalescence was observed again, which means that the surface of the surveyed boulders has been exposed (and been stable) since at least 1820 CE. Only in the rock glacier ridges closer to the headwall (stations H4LS-5 and H4LS-6), however, thalli did not coalesce, yielding dates from 1913/1914 CE, according to *Rhizocarpon geographicum* measurements, and 1866/1844 CE, according to the *Porpidia* cf. *soredizodes* ones. The stations in the ridges of the depression (from H4LS-7 to H4LS-9) yielded dates from 1932 to >1999 CE, according to *Rhizocarpon geographicum*, and from 1844 to 2002 CE, according to *Porpidia* cf. *soredizodes* species. In both cases, dates were always younger ages towards the cirque headwall.

4.5. Boulder displacement

The results obtained from boulders placed on stable areas in Hofsdalur cirques are summarized in Tables S9 and S10 and the spatial distribution can be seen in the maps in Figs. 9 and 10, which show:

(i) *Stable areas* (as they are not on ice-cored landforms). The mean horizontal displacement values range between 0.034 m yr^{-1} (1980–1994) and 0.017 m yr^{-1} (1994–2019; Tables S9 and S10). The boulders sampled for CRE dating hardly show any elevation difference in 1980, 1994 and 2019, with maximum values ranging between −0.5 and + 0.35 m (Table S6). Considering that these areas are in fact stable, we take these movement values as the uncertainty range for the boulder displacement.

(ii) *Cirque Hofs-1.* The debris-covered sector of the glacier showed a mean horizontal displacement for the period 1980–1994 of 1.63 m, which implies an average annual rate of 0.12 m yr^{-1} (Tables S9 and S10). This movement has increased over the period 1994–2019 to 0.15 m yr^{-1}. The highest rates (>0.25 m yr^{-1}) during both periods mainly occurred in the moraines closing the large intermediate depression (Fig. 9). Here, the displacement vector of the landform pointed towards the centre of the depression. Velocities at the centre of the debris covered sector are lower (0.05 and 0.15 m yr^{-1}), increasing slightly towards the frontal ridges (0.15–0.20 m yr^{-1}), where CRE samples were taken. In this case, the 5 m buffer analysis performed on each CRE sample (HEC-1, HEC-2 and HEC-3) showed velocity of 0.14 m yr^{-1} during 1980–1994, and 0.15–0.21 m yr^{-1} during 1994–2019 (Table S6). Similarly, horizontal displacement rates around the SHED and lichen stations were lower than 0.272 m yr^{-1} (Table 3 and Table S7). On the other hand, vertical displacement of the blocks of the debris-covered glacier evidence of a clear process of subsidence, particularly intense in the period 1994–2019 (Fig. 11). While the maximum elevation changes recorded in some blocks during 1980–1994 were −3.45 m, in 1994–2019 they increased to −17.39 m. The highest shrinking rates were recorded in

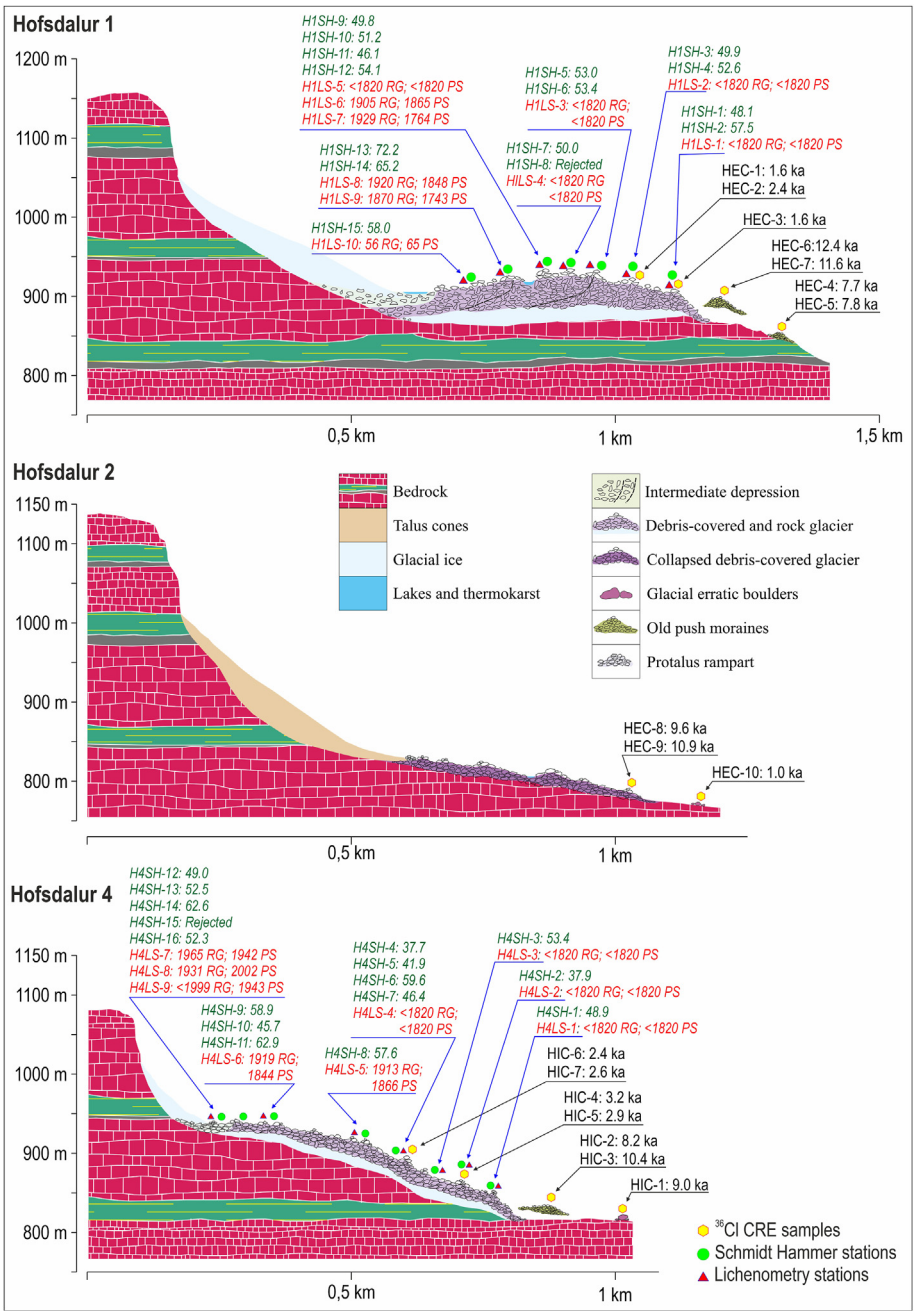

Fig. 5. Idealized longitudinal geomorphological profiles of cirques Hofs-1, 2 and 4 and the relative position and ages of the CRE, SHED sites and Lichenometry stations (LS)". The abbreviations "Rg" and "Ps" in lichenometry stations indicate the species *Rhizocarpon geographicum* and *Porpidia soredizodes* from which dates were returned, respectively. The inner structure of the profiles is speculative.

the large intermediate depression unit, linked to the displacement of the blocks from the upper parts of the recent moraine towards the bottom of the depression. On the other hand, moderate subsidence values between 2 and 5 m are found in most of the area. The ridges where the CRE samples were collected recorded a total sinking between −2.09 and −2.80 m during the over the period 1994–2019, while those where SHED was applied showed a generalized subsidence from 1980 to the present, with values ranging between −1.2 and −4.4 m (Tables 3 and 5, and Tables S6, S7).

(iii) *Cirque Hofs-2.* The comparison of horizontal displacement rates in 1980–1994 and 1994–2019 is indicative of the absence of movement in the collapsed debris-covered glacier, with mean displacements of only 0.04 m yr^{-1} and 0.02 m yr^{-1}, respectively (Table S9 and Fig. 9). Likewise, elevation changes recorded at the tracked blocks are generally close to the values observed at the stable ones, thus indicating high stability (Table S10 and Fig. 10).

(iv) *Cirque Hofs-3.* In this case, similar stability was observed in the small rock glacier. The mean horizontal displacement was 0.74 m (1980–1994) and 1.11 m (1994–2019), which accounts for movement rates of 0.05 and 0.04 m yr^{-1}, respectively.

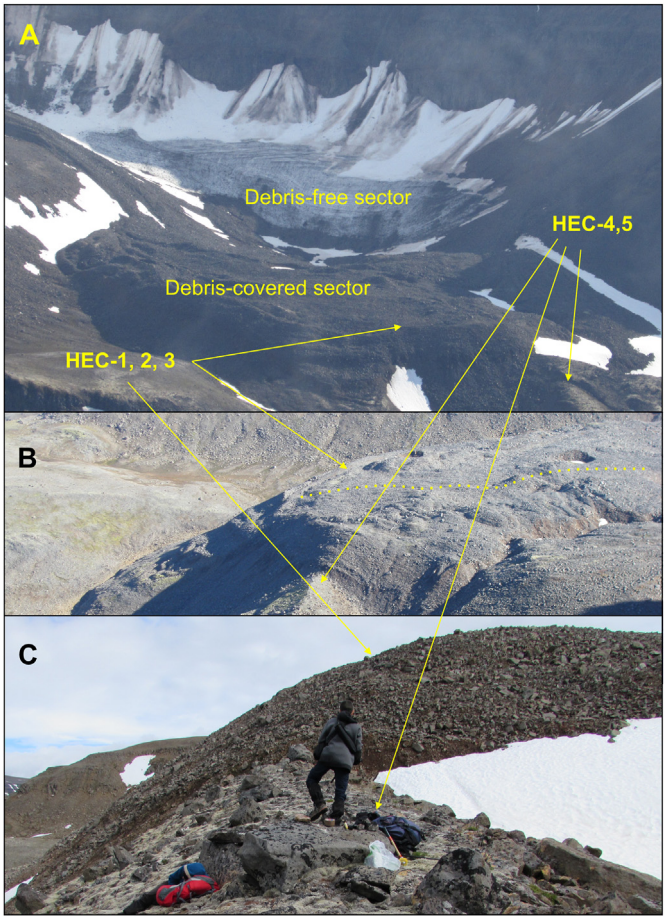

Fig. 6. Photos indicating the location of CRE samples in Hofs-1 cirque. (A) The cirque from the north, showing the push moraine, the debris-covered and debris-free sectors of the present glacier and the intermediate depression. (B) The debris-covered glacier from the west. The dotted line indicates the transect where the SHED and lichen stations are located. (C) The moraine and the end of the debris-covered sector.

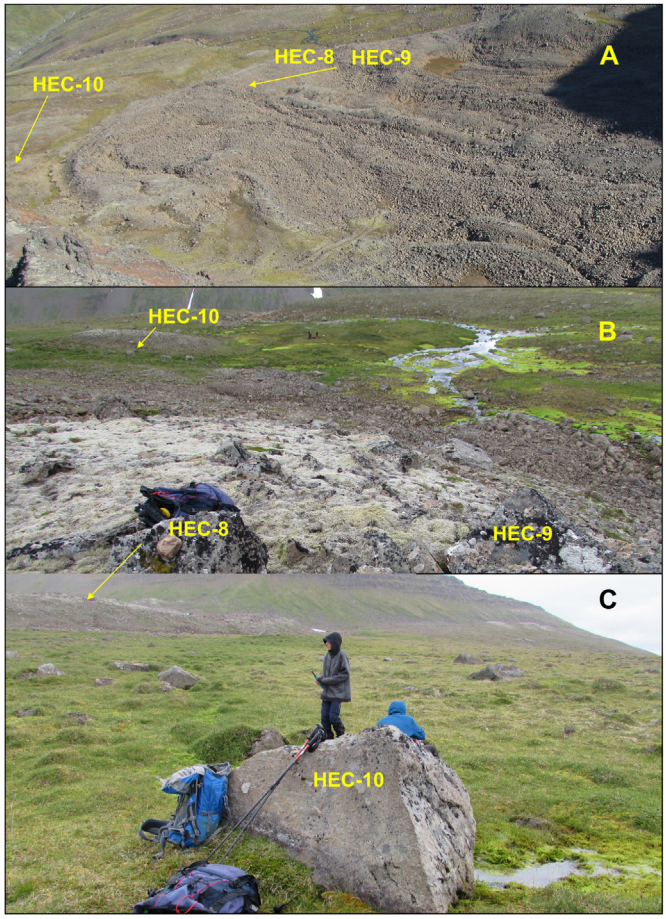

Fig. 7. Photos of Hofs-2 cirque showing the location of CRE samples. (A) The cirque from the west, showing the collapsed debris-covered glacier and hummocky moraine. (B) View of terminus from the south. (C) HEC-10 boulder and view from the north.

(v) *Cirque Hofs-4.* The rock glacier recorded mean horizontal displacements of 0.14 m yr^{-1} (1980–1994) and 0.12 m yr^{-1} (1994–2019), respectively (Fig. 9, Table S9). In addition, analysis of the elevation changes of the blocks showed a general sinking pattern for the entire rock glacier surface: in 1980–1994 the maximum negative value identified was −0.90 whereas in 1994–2019 the maximum reached −4.57 m (Table S10, Fig. 7). The ridges sampled on the rock glacier for CRE dating, lichenometry and SHED yielded velocities and sinking values close to the average (Table 4 and Tables S6, S7, S8). Indeed, movement rates from boulders with CRE samples in the moraines were similar to those of the stable blocks (Table S6).

4.6. Recent glacier surface changes, glacier reconstructions and ELA in Hofs-1

(i) *Recent glacier changes.* In Hofs-1 the debris-free sector has shrunk from 23.33 to 14.23 ha (−39%) over the 1980–2019

Table 6
Glacier longitude, expanse and volume evolution, calculated from reconstructions and DEM. Delta (Δ) is referred to the change regarding the stage 1. Glacial Equilibrium-Line Altitudes (ELAs) evolution calculated over Hofs-1 glacier through the application of the AAR and AABR method (see Fig. 12 for the extension of the glacier in the different stages).

Stage	Long. (km)	Δ (%)	Area (ha)	Δ (%)	Vol. (hm^3)	Δ (%)	ELA-AAR (0,67; m)	ELA-AABR (1,5 ± 0,4 m)
1	1.24	–	46.76	–	12.56	–	962	977
3	1.07	−13.71	39.47	−15.59	10.01	−20.31	980	990
4	0.94	−24.19	32.85	−29.75	7.91	−37.02	993	998
1980	0.79	−36.29	23.32	−50.13	4.94	−60.67	998	1008
1994	0.78	−37.1	22.82	−51.2	4.79	−61.86	997	1007
2000	0.78	−37.1	21.43	−54.17	4.39	−65.05	990	1000
2019	0.65	−47.58	14.23	−69.57	2.5	−80.1	976*	991*

Note: Equilibrium-Line Altitudes (ELAs) resulting from Accumulation Area Ratio (AAR, 0.67) and Area–Altitude Balance Ratio (AABR, 1.5) methods are expressed in m a.s.l. Asterisks indicate that such ELA values are excluded from the interpretation given that the lowering they represent is derived from hypsometric issues (generalized subsidence of the glacier surface) rather than climate events.

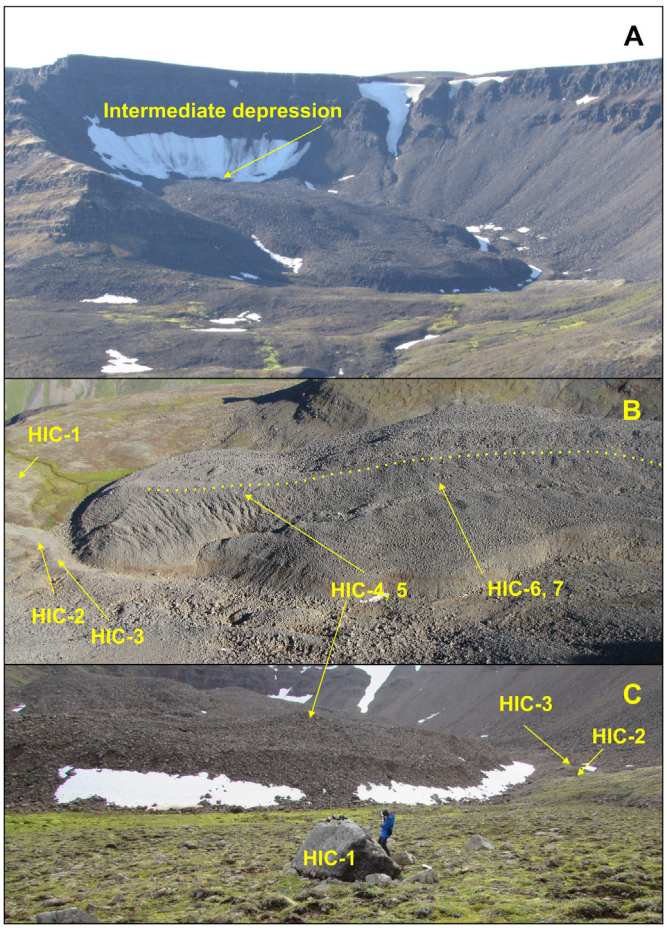

Fig. 8. Photos of Hofs-4 cirque. (A) The present glacier and push moraine, from the north. (B) The cirque from the west. The dotted line indicates the transect where the SHED and lichen stations are located. (C) The moraine and terminus of rock glacier. Locations of CRE samples are indicated in B and C.

period. The surface lowering of the debris-free glacier and the intermediate depression shows an average net thickness difference of −20.31 ± 1.76 m (Table 5 and Fig. 11), which accounts for a total loss of 4.71 ± 0.41 hm^3. The highest subsidence figures are concentrated in these sectors of the glacier. The subsidence is weaker in the debris-covered sector and the rock glacier, with an estimated total volume loss of 1.73 ± 0.64 hm^3 and an average thinning of −4.74 ± 1.76 m.

(ii) *Glacier reconstructions of older stages.* Glacier surface reconstructions in the different stages are shown in Fig. 12. For Stage 1 (maximum extent within the limits of the cirque) the glacier reached 1.24 km long and occupied an area of 46.76 ha, storing 12.56 hm^3 of ice. By 2019, these values had decreased to 0.65 km (−47.58%), 14.23 ha (−69.57%) and 2.5 hm^3 (−80.1%). Values for intermediate stages are listed in Table 6.

(iii) *ELA.* The ELA rose from 962 to 977 to 998–1008 m between Stage 1 and the year 1980, according to the AAR and AABR methods. Assuming that precipitation remained constant throughout the stages, together with a 0.66 °C lapse rate (Stötter et al., 1999; Fernández-Fernández et al., 2017), a minimum warming of 0.2–0.24 °C is estimated for this period. According to the glacier hypsometry changes, since 1980, the ELA decreased to 978 m in 2019 (Table 6 and Fig. 12).

5. Discussion

5.1. The evolution of the hofsdalur cirques throughout the holocene

A set of geomorphological units have been identified in the Hofsdalur cirques on the basis of their current morphology and dynamics, which allow to infer 4 glacial stages:

A) Initial occupation of the cirques by debris-free glaciers

All the cirques in Hofsdalur are enclosed by external push moraines. Based on their morphology, push ridges showing an absence of hummocks and of supraglacial till inwards, we deduced that they were deposited by debris-free glaciers. The ^{36}Cl dates are consistent with their chronostratigraphical position:

- In the Hofs-1 cirque, two moraine ridges were dated, the most external one at 12.0 ± 0.8 ka (n = 2) and the inner one at 7.7 ± 0.5 ka (n = 2).
- In Hofs-2, the most external erratic boulder of the cirque yielded an exposure age of 12.5 ± 1.0 ka.
- In Hofs-4, the most external moraine of the cirque returned an exposure age of 9.2 ± 0.7 ka (n = 3) (Fig. 13).

These CRE ages suggest that small debris-free glaciers occupied the bottom of the cirques at the transition from the Late Glacial to the early Holocene. For example, in 12.0 ± 0.8 ka, the glacier in Hofs-1 stored an ice mass of 12.56 Hm^3, with its ELA placed at ca. 960–980 m (Table 6).

B) Divergent evolution towards different landforms

(i) *Collapsed debris-covered glacier.* In Hofs-2 cirque the debris-free glacier evolved into a debris-covered one and collapsed by 10.2 ± 0.2 ka (n = 2) when the internal ice mass melted away (Table S6). Boulder displacement data confirm the present-day stability of this landform (Table S9).

(ii) *Frontal sector of the debris-covered area of the present glacier.* At Hofs-1 cirque, the front of the glacier evolved into a debris-covered glacier after 7.7 ± 0.5 ka (n = 2). At that time, in some sectors, the glacier advanced and overrode the older push moraine. Lichenometry data reveal that, despite the underlying ice core of glacial origin, boulders have remained stable for >250–300 years. The CRE ages confirm the pattern, pointing to stabilization occurring at 1.8 ± 0.3 ka (n = 3; Table S6, Fig. 13). The SHED at this sector yielded a mean R value of 50.0 ± 0.9 (n = 3). Before its transformation into a debris-covered one, the glacier of the Hofs-1 cirque had an ice mass of 12.56 Hm^3 of ice, with an ELA of 962/977 m. The values of horizontal boulder displacement obtained indicate low mobility over the last 30 years (<0.2 m yr^{-1}). In contrast, elevation changes have been more pronounced over the period 1994–2019 (−3.551 m yr^{-1}) than in 1980–1994 (−0.77 m yr^{-1}). Between 1980 and 2019, this entire sector underwent a general lowering trend that accounted for a total mass loss of 1.73 ± 0.64 Hm^3 and an average thinning of 4.74 ± 1.76 m. All these results show evidence that the frontal sector remains in a stagnant stage, with no glacial flow any longer.

(iii) *Active rock glaciers.* In Hofs-3 and 4 cirques, the glaciers transformed into rock glaciers after 9.2 ± 0.7 ka (n = 3). Hofs-3, due to the small size of its landforms, was not included in

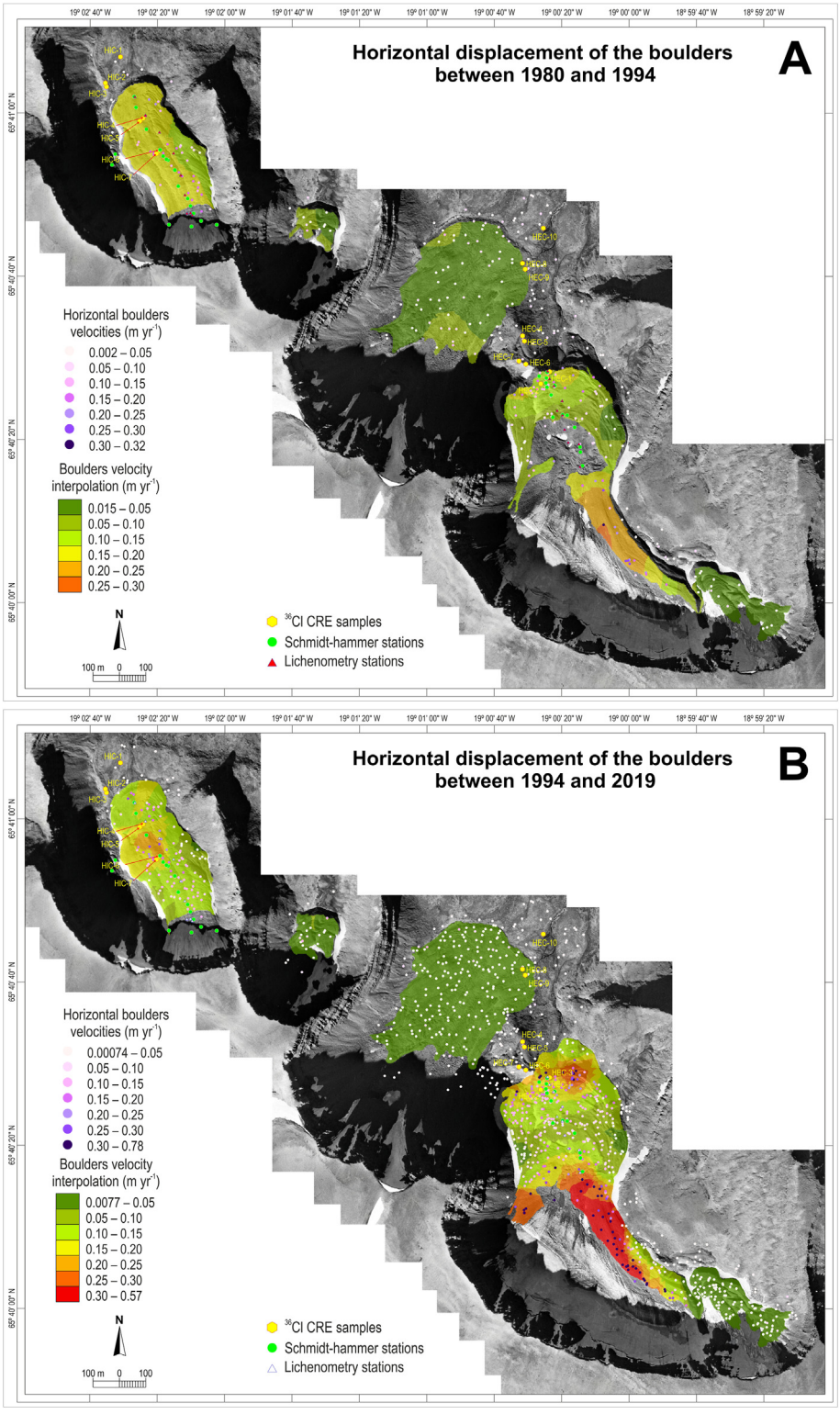

Fig. 9. Interpolated velocity field map showing rates of surface boulder movement (horizontally) for the periods 1980–1994 (A) and 1994–2019 (B).

this analysis. Lichenometry dates show that the surface boulders of Hofs-4 rock glacier have remained stable for more than 250–300 years. CRE ages confirm that this stability was achieved by 2.8 ± 0.4 ka (n = 4). The SHED indicated R values of 49.1 ± 1.1 (n = 9) for this sector. The CRE and SHED results from Hofs-1 and 4 cirques followed similar pattern, with CRE ages of 2–3 ka and R values of 50 ± 1. Surface boulder displacements at the Hofs-4 rock glacier show a very slow movement over the last 30 years, with average velocity rates <0.15 m yr^{-1}. The average subsidence of the landform boulders increased over the last 25 years (−1.852 m; 1994–2019 vs −0.267 m; 1980–1994). The

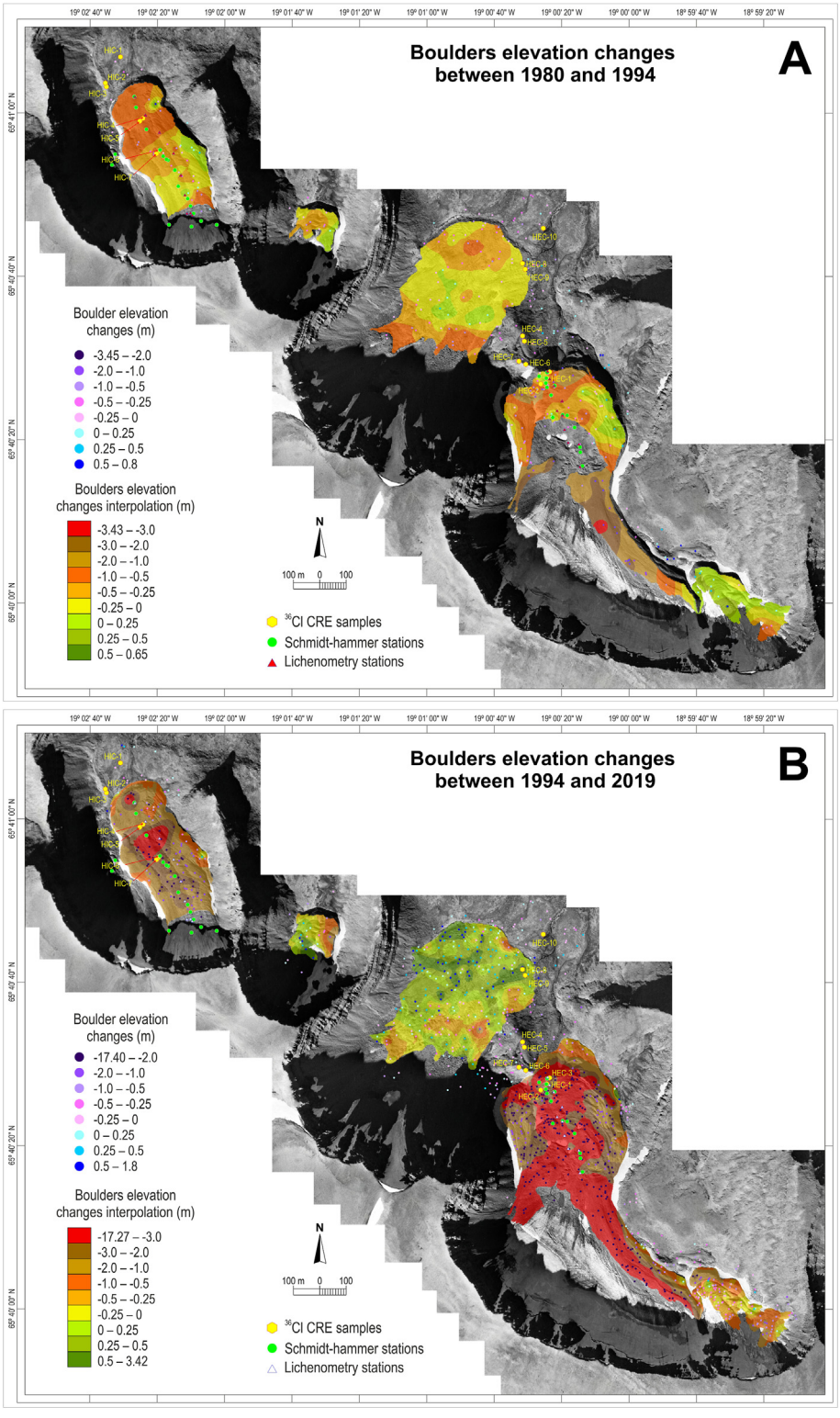

Fig. 10. Boulder elevation changes and interpolated elevation differences map for the periods 1980–1994 (A) and 1994–2019 (B).

results show that the Hofs-4 rock glacier is undergoing a stagnant phase, with subsidence prevailing over a very limited flow.

C) Advance of new small debris-free glaciers at the headwall

In Hofs-1 and 4 cirques, the debris-covered sectors and the rock glacier show very weak geomorphological dynamics. However, in the upper parts of these cirques, the debris-free glacier sectors behave as independent glaciers. Field geomorphological observations revealed that the debris-covered sector of the Hofs-1 glacier and the Hofs-4 rock glacier are overlapped by younger push

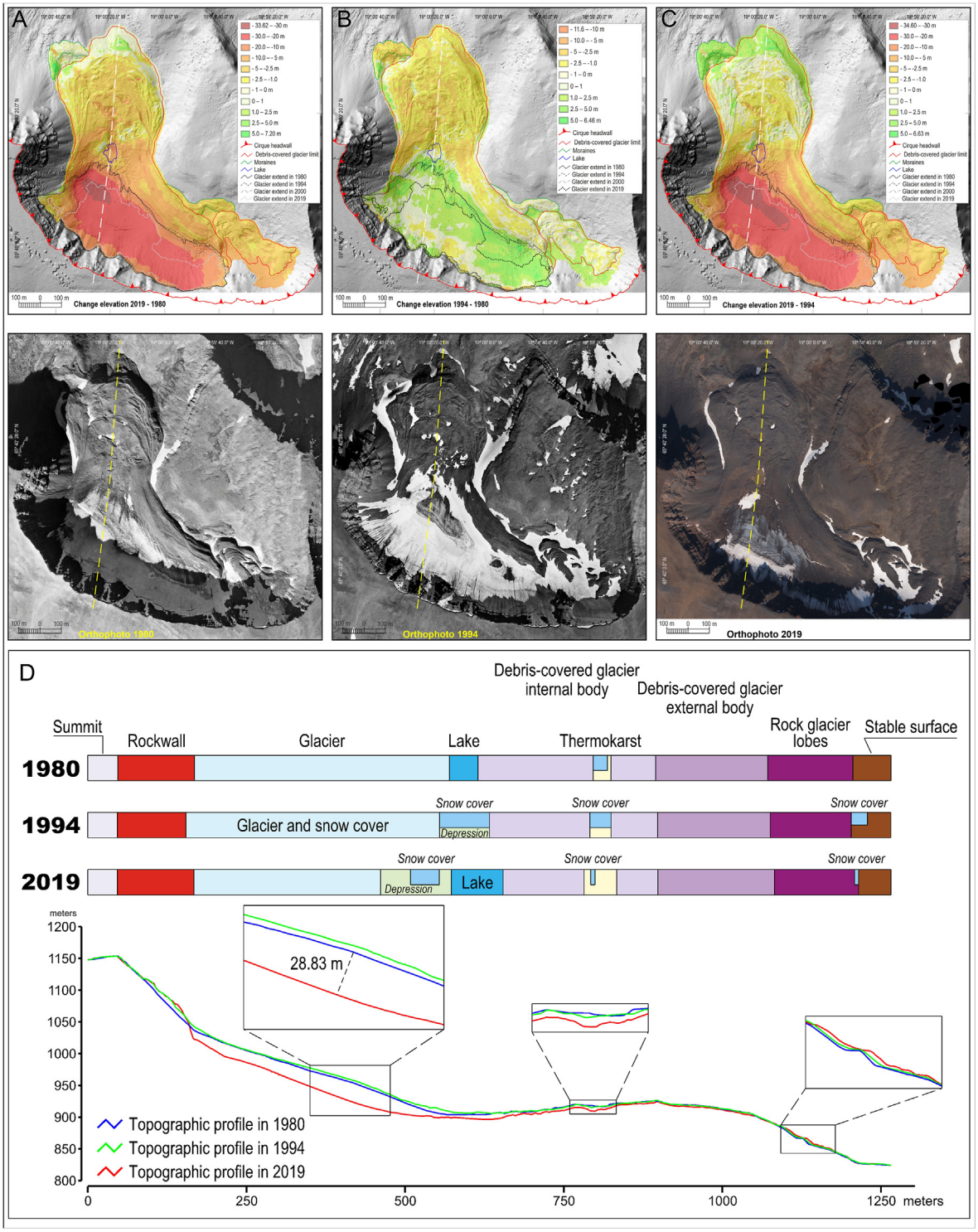

Fig. 11. Differences in elevation models for Hofs-1 cirque for the periods: (A) 1980–2019; (B) 1980–1994 and (C) 1994–2019, with orthophotos for 1980, 1994 and 2019. (D) Long profiles for 1980, 1994 and 2019, and proportions of different surface types.

moraines deposited by the debris-free glaciers in these cirques (Figs. 3, 6 and 12). Lichenometric results show a discrepancy between the moraine ages based on the species *Rhizocarpon geographicum* (1904–1923 CE) and those obtained for the *Porpidia soredizodes* (1764–1870 CE) in Hofs-1 and those inferred for Hofs-4 (1913/1914 CE and 1866/1844 CE, respectively). This is probably due to local factors that condition different lichen growth rates than those obtained in neighbouring glaciers (Hannesdóttir et al., 2020; Fernández-Fernández et al., 2020), producing inconsistent results. In any case, lichenometry data indicate that these moraines were deposited during the last 250 years, i.e. from the mid-18th century to the early 20th century. Two generations of these younger push moraines in Hofs-1 allowed estimation of the volume of this glacier for two stages, with 10 and 8 Hm^3, which means reductions of 20.3

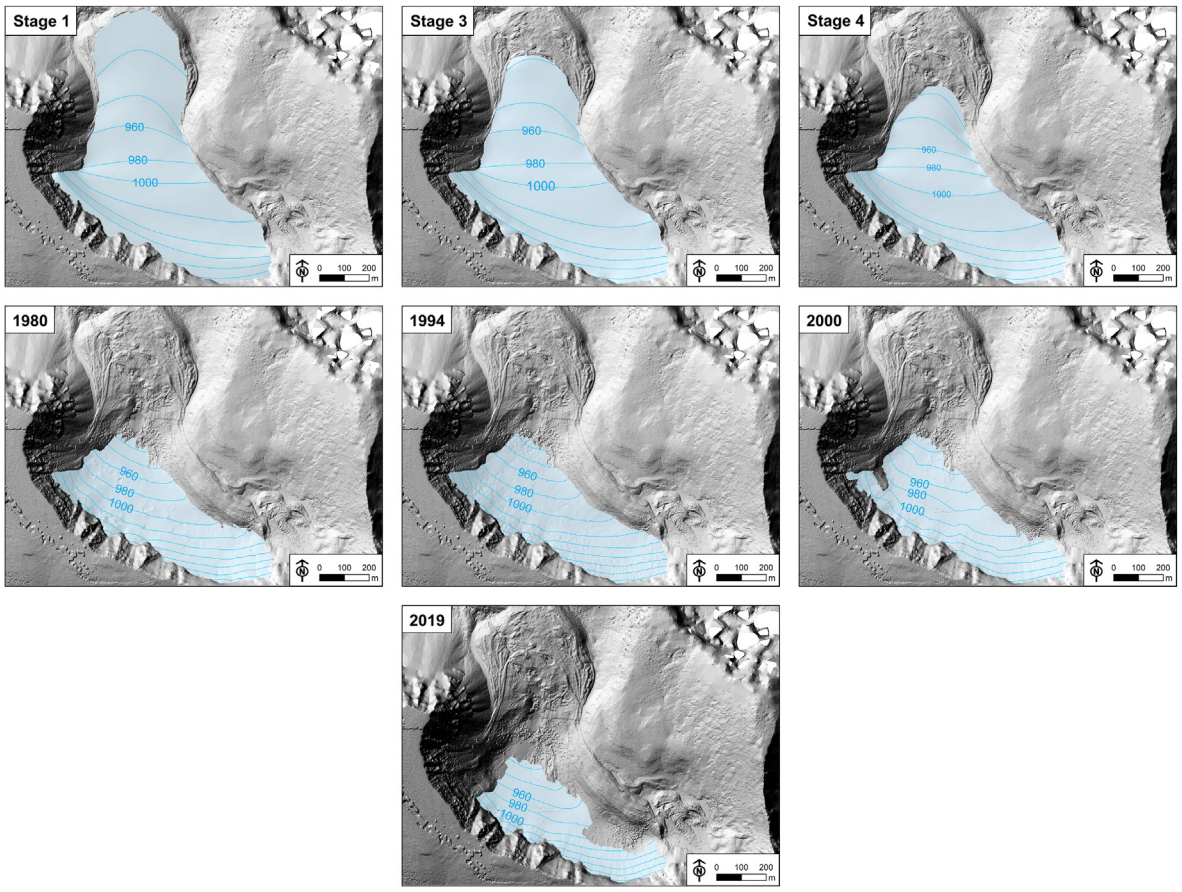

Fig. 12. Three-dimensional glacier reconstructions of Hofs-1 glacier during different stages.

and 37.0%, respectively, in relation to the maximum extent stage (Fig. 12). The ELAs for these two stages were estimated as 980 and 998 m, respectively.

D) Retreat of the debris-free glaciers

After a number of advances, the small debris-free glaciers retreated and uncovered intermediate depressions in Hofs-1 and 4 cirques. This retreat of the glacier front caused instability of the opposite front of the debris-covered sector, both in the glacier in Hofs-1 cirque and in the rock glacier sector of Hofs-4 cirque, resulting in the greatest horizontal displacement rates and the greatest vertical lowering of the boulders during the last century. Most of these displacements followed an opposite direction to the general pattern of glacial flow. In Hofs-1 cirque, the average total lowering was 20.31 ± 1.76 m, with maximum values of −33.62 m. The SHED results in these ridges indicate high R-values of 68.4 ± 0.8, (n = 3), indicative of surfaces that have stabilized recently. This is confirmed by lichenometric data that yielded ages from 1932 to 2002 CE, depending on the species. During recent decades, the debris-free sectors of the glaciers in the upper parts of the cirques have shown typical glacial dynamics. The glaciers kept shrinking and the depression in front continued to widen, favouring the formation of lakes within the depression (Fig. 3). This process has accelerated in recent decades. In fact, the Hofs-1 glacier has lost half of its volume since 1980: it currently stores 2.5 Hm^3 of ice, i.e. 80% less compared to its maximum extent just after 12.0 ± 0.8 ka. Currently, the ELA is located above 990 m.

In summary, each of the glaciers within the Hofsdalur cirques evolved into different landforms; but two of them reformed as debris-free glaciers in the last few centuries. It seems that the local morphological and topographical conditions of each cirque are crucial to explain the different spatio-temporal patterns in their geomorphological evolution.

5.2. The divergent evolution of glacial landforms during the last deglaciation in the Tröllaskagi Peninsula

The comparison of the results obtained in the Hofsdalur cirques (Hofs 1–4) with those obtained in the cirques of nearby valleys, namely Hóladalur valleys to the north (Fernández-Fernández et al., 2020) and Héðinsdalur valley to the south (Palacios et al., 2021), allows us to identify some common patterns in their glacial evolution (Fig. 15 and Figure S6, S7, S8):

(i) *Debris-free glaciers occupied the Tröllaskagi cirques during the Younger Dryas (YD) and receded rapidly during the Holocene transition* (Fig. 15, A, F, J).

Currently, most of the 160 glacial cirques of Tröllaskagi contain debris-covered and rock glaciers (Caseldine and Stotter, 1993). Indeed, in all of them where CRE dating has been applied, results suggest that these cirques were initially occupied by debris-free glaciers that left scattered erratic boulders and push-moraine ridges, deposited during advances or stabilizations of the glacial fronts with a limited debris load.

Generally, CRE dating reported similar ages for the formation of these landforms that occurred after deglaciation of the nearby

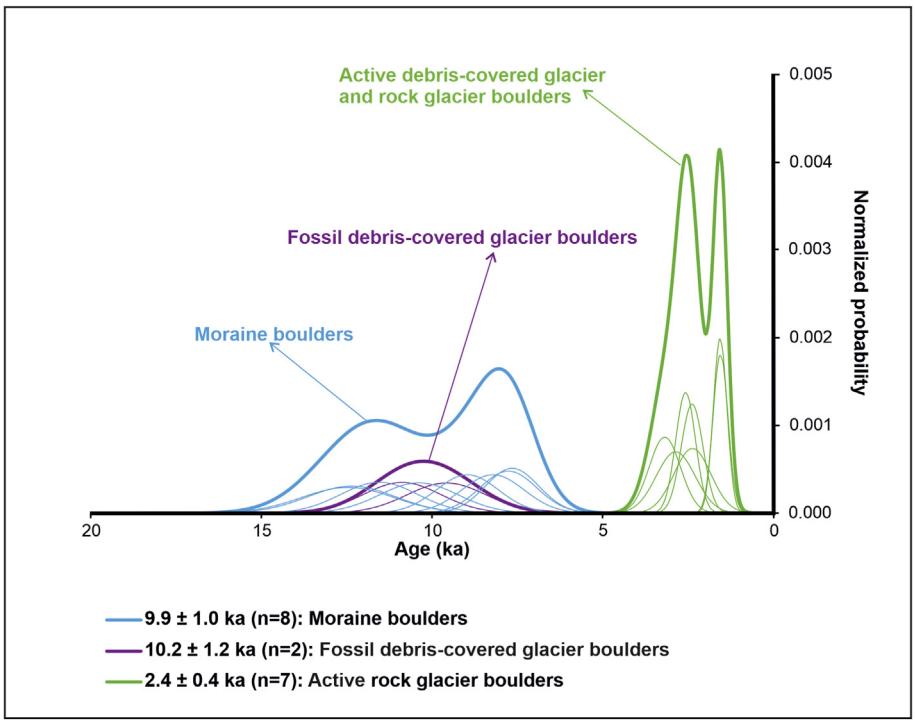

Fig. 13. Probability density plots of CRE ages for different chronostratigraphic units in the Hofsdalur cirques in relation to different boulder locations.

Víðinesdalur valley, 16.3 ± 1.1 ka ago (Fernández-Fernández et al., 2020). The ages of the push moraines that formed at the mouths of the cirques in the Hofsdalur valley are of 10.2 ± 1.2 (n = 8) ka and 10.1 ± 0.7 ka (n = 11) if we included the Hóladalur samples, corresponding between the end of the YD to the early Holocene (Fig. 14; Fernández-Fernández et al., 2020). Around 12 ka (during the YD), one of the glacial outlets of the Iceland Ice Sheet, channelled through the Skagafjörður fjord, reached its maximum extent. Subsequently, by ~10 ka ago, this outlet glacier had retreated so that to the size of the IIS was very close to that of the present-day Hofsjökull ice cap, extending across the highlands in the central part of the island (Andrés et al., 2019). Glaciers expanded throughout northern Iceland during the YD (Pétursson et al., 2015), under the extremely cold and dry climate conditions (Rundgren 1995, 1999).

(ii) *Glaciers became debris-covered glaciers and rock glaciers, but their ice-cores melted rapidly and collapsed during the Early Holocene in low-altitude cirques and lower cirque sectors* (Fig. 15, B, G, K).

In the Hofs-2 cirque, whose bottom is the lowest (820 m), the debris-free glacier evolved into a debris-covered one 12.5 ± 1.0 ka ago, and the front collapsed by 10.2 ± 0.2 ka. A similar pattern is found in other Icelandic low-altitude cirques, such as in Fremri-Grjótárdalur valley (830 m), where rock glaciers formed just after the onset of deglaciation and collapsed by 10.5 ± 1.0 ka (Fig. 14; Fernández-Fernández et al., 2020). A similar process occurred in a ca. 100 m higher part of the same cirque, with a stabilization at 9.5 ± 1.0 ka (Fig. 14; Fernández-Fernández et al., 2020). In contrast, in the Hofs-1 cirque at 900 m, the debris-free glacier persisted until 7.7 ± 0.5 ka as indicated by the ages of its outer moraines. Similarly, an analogous pattern was observed in the upper sector of the Héðinsdalur cirque, at an altitude of 950 m, where a push-moraine was dated at 6.6 ± 1.0 ka (Palacios et al., 2021). These ages fall within the range of the Holocene Thermal Maximum (HTM, 10–6 ka BP; Renssen et al., 2012). There is documented evidence of glacier disappearance during the HTM in Central Iceland (Geirsdóttir et al., 2009, 2019; Larsen et al., 2012). In contrast to those low relief environments, the alpine setting in the Tröllaskagi Peninsula conditioned a significant geomorphological response: the shrinking glaciers triggered paraglacial processes on their surrounding walls, which supplied debris onto the ice surface and partly insulated the glacier from air temperature oscillations and solar radiation (Humlum, 2000).

(iii) *Following the HTM, debris-covered glaciers and rock glaciers still preserved their ice-cores, but stagnated* (Fig. 15, C, H, L).

After the HTM, all debris-free glaciers in Hofsdalur area evolved to debris-covered or rock glaciers, as happened also in the Hóladalur valley. However, their flow was limited, and they soon became stagnant enough to allow their boulders (and surfaces) to be uninterruptedly exposed to cosmic rays (Tanarro et al., 2019; Campos et al., 2019). The exposure ages of these boulders are 1.8 ± 0.3 ka, in the case of the debris-covered glacier Hofs-1, and 2.8 ± 0.4 ka, in the rock glacier of Hofs-4. The stabilization ages in Hofsdalur are of similar age as the front of Héðinsdalsjökull rock glacier (Palacios et al., 2021), but about 3–4 ka younger than those of the active rock glaciers in Fremri-Grjótárdalur cirque and for the debris-covered glacier Hofsjökull with a mean age of 6.0 ± 0.3 ka (Fig. 14; Fernández-Fernández et al., 2020). The Hofsdalur ages fall within the Neoglaciation in Iceland, when a series of significant glacial advances in Southern, Central and North-Western Iceland started at 5 ka (Kirkbride and Dugmore, 2006, 2008; Striberger et al. 2011, 2012; Geirsdóttir et al., 2018, 2019), as a consequence of regional climate cooling and ELA lowering (Andersen et al., 2004; Geirsdóttir et al., 2009, 2013, 2018, 2019). The debris-covered and rock glaciers of Tröllaskagi do not show any evidence of reactions to Neoglacial cold pulses which did, however, allow for survival of

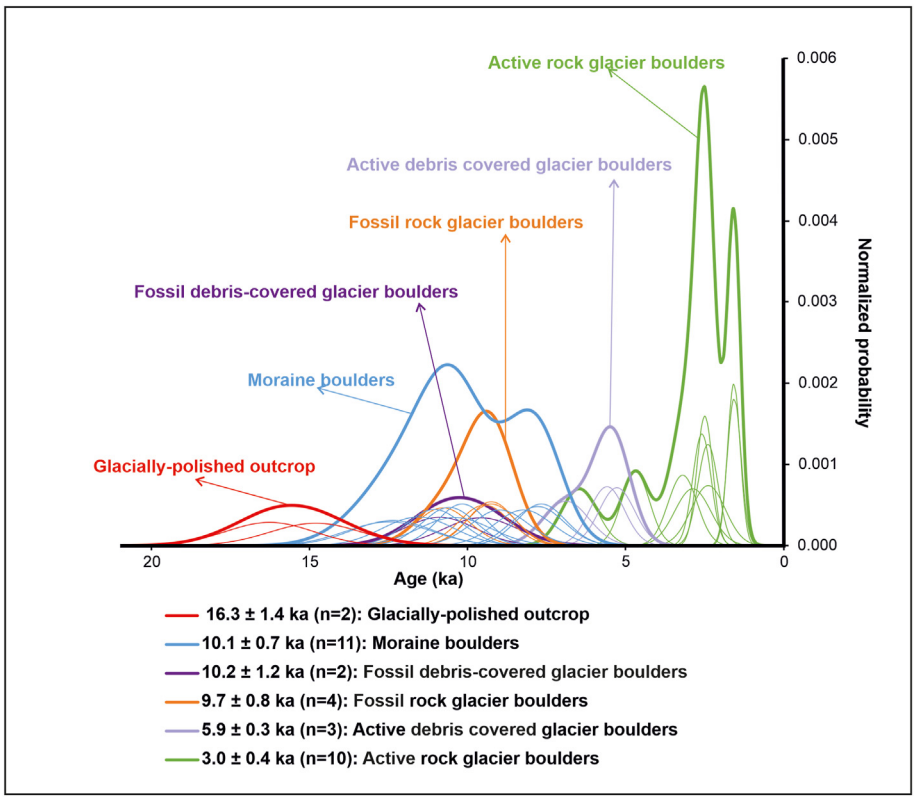

Fig. 14. Probability density plots of CRE ages for different chronostratigraphic units in the Hofsdalur cirques together with the results obtained in similar geomorphological units in the Hóladalur cirques (Fernández-Fernández et al., 2020).

their ice cores. On the contrary, the few cirques in Tröllaskagi hosting debris-free glaciers preserve a long series of Neoglacial moraines indicative of advances at 4.7, 4.2, 3.2–3.0, 2.0, 1.5 and 1.0 cal ka BP (see synthesis in Stötter et al., 1999), and at 1.6 and 1.3 ka using CRE dating (Fernández-Fernández et al., 2019).

(iv) *During the Little Ice Age (LIA), the debris-free sectors of the glaciers behaved as independent glaciers* (Fig. 15, D, M).

During the LIA, the debris-free sectors of the glaciers overlapped and pushed the debris covered sectors or the rock glaciers in Hofsdalur cirques, forming younger push-moraines over them. Comparable moraines have been also described in the Hóladalur and Hofsjökull cirques, where the upper sectors of debris-free glaciers have been suggested to be independent glaciers (Tanarro et al., 2019; Campos et al., 2019: Fernández-Fernández et al., 2020).

Such moraines have also been observed in Héðinsdalsjökull valley, where lichenometric dating yielded results corresponding to the beginning of the 19th century (Palacios et al., 2021), similar to those obtained in this work. These ages are in good agreement with the LIA being the greatest cooling of the second half of the Holocene in Iceland (Ogilvie and Jónsson, 2001; Miller et al., 2010; Larsen et al., 2011, 2012). Traditionally, LIA glaciers have been suggested to reach their maximum extent in the south and the centre of Iceland between the 18th and 19th century, based on lichenometric dating (Kirkbride and Dugmore, 2006, 2008; Chenet et al., 2010). Indeed, this dating approach also revealed glacial advances during several phases of the late LIA in the debris-free glaciers of a few cirques in Tröllaskagi (Caseldine and Cullingford, 1981; Caseldine and Stotter, 1993; 1985; Kugelmann, 1991; Häberle, 1991; Caseldine and Stotter, 1993). However, ^{36}Cl CRE dating applied in the Vesturdalur and Austurdalur valleys (central Tröllaskagi) revealed an earlier maximum LIA expansion dating back to the 15th and 17th centuries, for the first time in Tröllaskagi (Fernández-Fernández et al., 2019). In those valleys, several minor glacier advances or standstills throughout the 19th century were documented: in the decades of 1800s, 1830s, 1840s, 1860s and 1890s (Fernández-Fernández et al., 2019). Our results, together with those in the Hóladalur and Héðinsdalur valleys, show that while the debris-covered and rock glaciers remained stagnant during the LIA, the debris-free glaciers advanced, as did others in Tröllaskagi, but the debris-free glaciers encountered the barrier of ice-debris formations that they eroded and overtopped.

(v) *After the LIA, the debris-free sectors of the glaciers retreated and an intermediate depression formed between their fronts and the ice-debris formations* (Fig. 15, E, I, N).

There are large intermediate depressions between the fronts of the upper debris-free glaciers and the debris-covered sector of the Hofs-1 cirque as well as the rock glacier of Hofs- 4. Similar depressions have been found in all cirques in the Hóladalur and Héðinsdalur valleys. In all cases, they are considered to be the most active sectors of the different landform complexes, with strong subsidence rates and frequent occurrence of massive lobate slides, mostly descending towards the centre of the depression from the ice-debris formations, in the opposite direction to glacier flow (Tanarro et al., 2019; Campos et al., 2019: Fernández-Fernández et al., 2020). Since the beginning of the 20th century, the few debris-free glaciers of Tröllaskagi underwent a general retreating trend, only interrupted by several advances in the 1910s, 1950s and from the mid-1980s to the mid-1990s (Fernández-Fernández et al., 2017, 2019). Some of latter advances have been detected in Hofs-1 and also in Héðinsdalsjökull (Palacios et al., 2021). This shows that

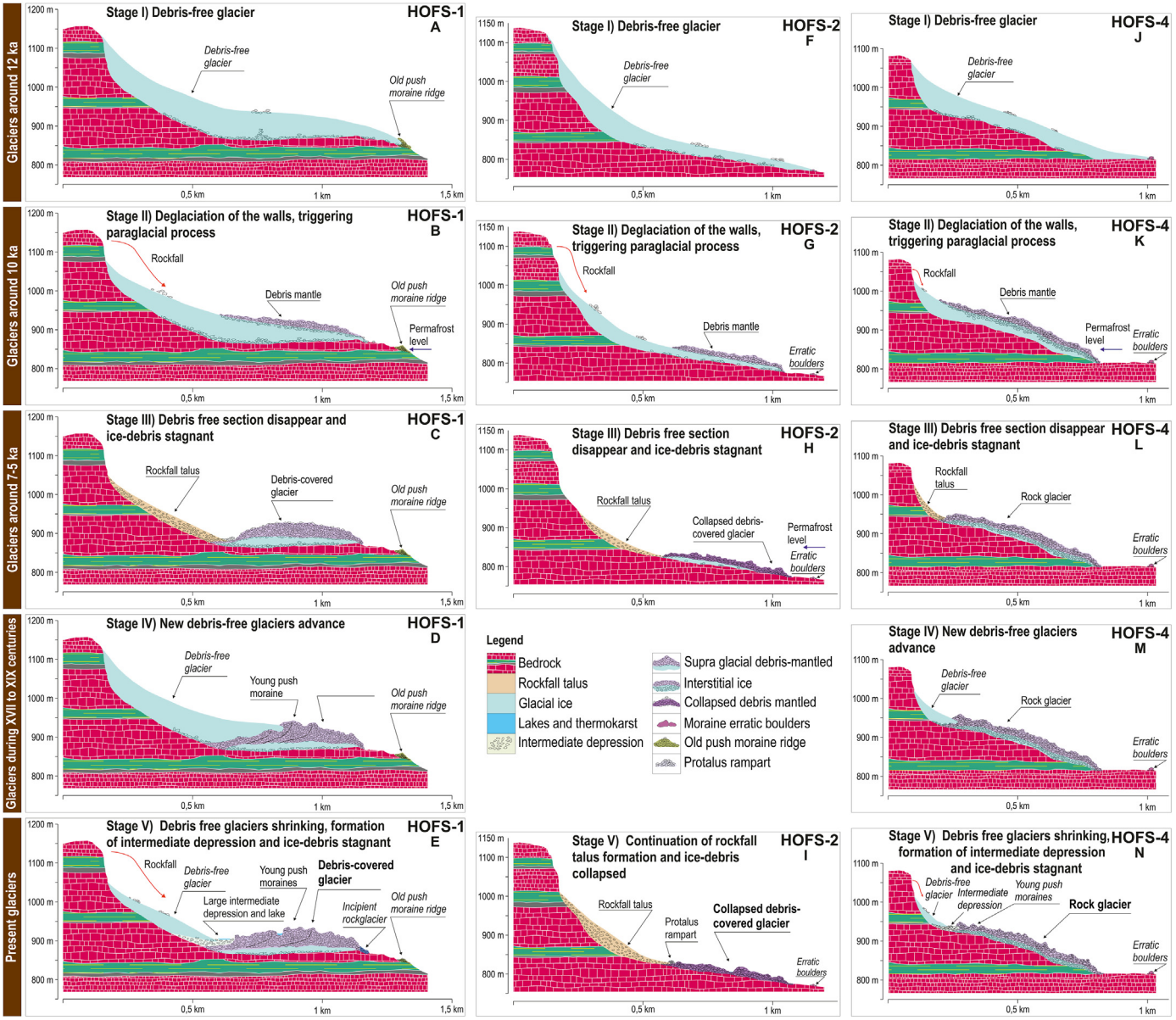

Fig. 15. Idealized model illustrating the proposed evolution of the glaciers in Hofsdalur 1, 2 and 4. During the YD (Stage 1), debris-free glaciers (A, F, J) occupied the cirques and deposited the older push moraines. Then deglaciation during the Early Holocene (Stage II: B, G, K) triggered paraglacial processes at the walls that supplied high volumes of debris falling onto the shrinking glaciers, leading to their transformation into debris-covered glaciers (Hofs-1 and Hofs-2; B, G) and a rock glacier (in Hofs-4 cirque; K), all with limited retreat given the insulating effect of the debris mantle. The deglaciation continued, and during the HTM (Stage III) the debris-free glaciers at the headwall sectors of the cirques disappeared (C, H, L); the front of the debris-covered glaciers and the rock glacier remained stagnant or even started collapsing (Hofs-2; H). By the LIA (Stage IV), new glaciers formed at the headwall sector of cirques Hofs-1 and Hofs-4 and advanced over the debris-covered (D) glacier and the rock glacier (M) derived from Stage II, overlapping them. And finally, following the end of the LIA (Stage V), the new debris-free glaciers at the cirque headwall retreated, leaving an intermediate depression on the surface of the debris-covered glacier (Hofs-1; E) and the rock glacier (Hofs-4; N), which are being affected by an intense subsidence process linked to the melting of the inner ice core, or even collapsing completely (Hofs-2; I).

these glaciers, behind the stagnant debris-covered glacier sectors, still behave as independent debris-free ones. On the other hand, the prevailing process detected in Tröllaskagi currently, in both rock glaciers and debris-covered glaciers, is their progressive subsidence, accompanied by the formation of thermokarst depressions (Tanarro et al., 2018, 2019).

The ELA of Hofs-1 glacier was about 100 m lower than those estimated for the larger glaciers Héðinsdalsjökull and Tungnahryggsjökull (Palacios et al., 2021; Fernández-Fernández et al., 2020) throughout the different stages of their evolution. In fact, the difference between the ELA of this cirque during the YD and the current one is very limited (from 970 to 990 m according to the model which indicates a maximum difference), which may be due to the topographic conditions of the cirque.

5.3. *The relevance of the divergent glacier evolution in tröllaskagi in a global context*

Present studies in Hofsdalur and previous studies in Hóladalur, Héðinsdalur and Grjótárdalur (Palacios et al., 2021; Fernández-Fernández et al., 2020; Tanarro et al., 2019) indicate that during the Holocene most of the Tröllaskagi glaciers evolved into debris-

covered glaciers and rock glaciers, and few remain as debris-free glaciers. But, what is the origin of such a divergent evolution?

An accurate analysis of the most important debris-free glaciers in Tröllaskagi highlighted a number of common characteristics: they are large, and their headwall source areas are completely (or almost) covered by ice, with a very limited wall surface from which supraglacial debris can be supplied (Andrés et al., 2016). These are the cases of the Gljúfurárjökull (Fernández-Fernández et al., 2017), Barkárdalsjökull (Häberle, 1991); Þverárjökull (Kugelmann, 1991) and the two nearby Tungnahryggsjökull valleys (Fernández-Fernández et al., 2019). Our results thus suggest that in most cirques in Tröllaskagi, post-YD glacial retreat under vertical and unstable walls (Whalley et al., 1983) triggered paraglacial processes that favoured the transformation of glaciers into debris-covered glaciers and rock glaciers. This has also been observed in other high or rugged mountains (Hambrey et al., 2008; Janke et al., 2013, 2015; Berthling, 2011; Monnier and Kinnard, 2015, 2016; Rowan et al., 2015; Anderson et al., 2018; Jones et al., 2019; Knight et al., 2019). It is noteworthy that these glacier transformations are very rapid and may occur within only a few hundred years (Linge et al., 2020).

While the debris-free glaciers reacted quickly and clearly to the climatic fluctuations throughout the Holocene with advances or retreats (Caseldine, 1985; Häberle, 1991; Kugelmann, 1991; Fernández-Fernández et al., 2017, 2019), the debris-covered glaciers underwent a more complex evolution: climatic changes themselves and the cirque floor elevation activated the paraglacial processes, in relation to fluctuations of permafrost conditions (Spreafico et al., 2021; Kääb et al., 2021).

Moreover, in cirques with moderate debris supply, glaciers tended to evolve into debris-covered glaciers, whereas in cirques with higher debris mobilization, glaciers gradually transformed into rock glaciers (Fig. 15; Berthling, 2011; Monnier and Kinnard, 2015; 2016; Janke et al., 2013, 2015). The activity of these landforms depends on their position in relation to the lowest level of permafrost, which in Northern Iceland is currently placed at around 900 m (Lilleøren et al., 2013; Etzelmüller et al., 2020). Thus, in cirques whose floor is below the regional permafrost level, these landforms collapse soon after their formation, as has been observed in Hofs-2, Héðinsdalsjökull (Palacios et al., 2021) and Fremri-Grjótárdalur (Fernández-Fernández et al., 2020).

During the HTM most glaciers in Iceland probably disappeared (Geirsdóttir et al., 2009, 2019; Larsen et al., 2012), whereas in Tröllaskagi glaciers transformed into debris-covered glaciers and rock glaciers, due to the very active paraglacial processes prevailing in most of the cirques (Deline et al., 2015; Anderson and Anderson, 2016; Mayr and Hagg, 2019). The fact of being located well above the regional permafrost level favoured preservation of ice, insulated by the debris mantle during this warm period (Lilleøren et al., 2013; Etzelmüller et al., 2020). But soon after deglaciation of the rock walls, there was a drastic decrease in the debris supply from the walls (Mercier et al., 2013; Cossart et al., 2014; Decaulne et al., 2016; Sæmundsson et al., 2018; Morino et al., 2019); these debris-covered glaciers and rock glaciers lost their flow and transformed into landforms that remain stagnant at present. This process has been reported from many other polar and mountain areas worldwide (Potter et al., 1998; Janke et al., 2013; Emmer et al., 2015; Anderson et al., 2018; Tanarro et al., 2019; Storni et al., 2020; Ferguson and Vieli, 2020).

These debris covered glacier and rock glacier landforms can be stable enough to uninterruptedly accumulate cosmogenic isotopes on the same surface of the boulders, which make it possible to determine their age of stabilization (Mackay and Marchant, 2016; Crump et al., 2017; Charton et al., 2020, 2021; Scherler and Egholm, 2020; Fernández-Fernández et al., 2020; Amschwand et al., 2021). At the same time and in the same cirques, the debris-free glacier sectors were separated from the ice-debris landforms and behaved as independent debris-free glaciers, very sensitive to climatic changes (Fig. 15). This is shown in their significant advance during the LIA and the subsequent fluctuations recorded over the last two centuries, similar to the other debris-free glaciers of Tröllaskagi, such as Héðinsdalsjökull (Palacios et al., 2021).

6. Conclusion

Our results show that the cirques in the Tröllaskagi peninsula are a natural laboratory for understanding and monitoring the transformation of debris-free glaciers into debris-covered glaciers and rock glaciers. Although this process has accelerated progressively in recent decades at global scale, it is still poorly understood. The results obtained in the Hofsdalur cirques are consistent with those obtained in other cirques in Tröllaskagi, as in Hóladalur and Héðinsdalur. In this case, their proximity and great evolutionary variety have allowed us to find some of the keys to understand the divergence of the glacier evolution during deglaciation.

During the YD (12.9–11.7 ka) the Tröllaskagi cirques, whose landforms have been dated by CRE methods, hosted debris-free glaciers. At early Holocene, these glaciers started to retreat. Some cirques might have hosted debris-free glaciers throughout the Holocene, which advanced and retreated in response to climate variability. But in most cirques, the intensity of paraglacial readjustment of the cirque slopes and the altitude of the cirque bottom determined the transformation of the glaciers into debris-covered glaciers or rock glaciers, as well as the early collapse or survival of their ice cores until the present day. In any case, the HTM promoted the stagnation of these ice-debris formations. Thereafter, the upper sectors of these glaciers, receiving a lower debris-supply from the headwalls since the HTM, behaving as independent debris-free glaciers, even overlapping the debris-ice formations in front of them during LIA glacial advances. With the onset of the current warming phase, the upper debris-free glaciers retreated and left an intermediate depression between their fronts and the ice-debris formations, which are the most geomorphologicaly active sectors today, in terms of displacement and subsidence. The current strong warming also affects the ice-debris formations, accelerating their melting and subsidence processes.

Declaration of competing interest

The authors declare that they have no known competing financial interests or personal relationships that could have appeared.

Acknowledgements

This paper was funded by the project PR108/20-20 (Santander Bank-UCM Projects) and Nils Mobility Program (EEA GRANTS), and with the help of the High Mountain Physical Geography Research Group (Universidad Complutense de Madrid). We thank the Icelandic Association for Search and Rescue, the Icelandic Institute of Natural History, the Hólar University College, David Palacios Jr. and María Palacios for their support in the field. José M. Fernández-Fernández is funded by a postdoctoral grant supported by the NUNANTAR project (02/SAICT/2017–32002; Fundação para a Ciência e a Tecnologia, Portugal). Marc Oliva is supported by the Ramón y Cajal Program (RYC-2015-17597) and by the Research Group ANTALP (Antarctic, Arctic, Alpine Environments; 2017-SGR-1102) funded by the Government of Catalonia. The ASTER national facility (CEREGE, Aix en Provence, France) is supported by the INSU, CNRS and the ANR through the “Projets thématiques d'excellence”

program for the “Equipements d'excellence” ASTER-CEREGE action and IRD. We thank the comments and suggestions of Dr. Ian S. Evans and anonymous reviewer, which have considerably improved the quality of the manuscript.

Author contributions

All authors have been involved in the investigation presented in this work:

Luis M. Tanarro, coordination of the all phases of the research and writing of a first draft of the manuscript, leading the fieldwork, geomorphological analysis, sampling and data processing. David Palacios, help in the coordination of the all phases of the research and writing of a first draft of the manuscript, leading the fieldwork, geomorphological analysis, sampling and data processing. José M. Fernández-Fernández. Laboratory tasks (sample processing, exposure age calculations) and contribution to the writing and revision of the manuscript. Nuria Andrés. Geomorphological fieldwork, geomorphological cartography data processing, geomorphological cartography and collaboration in the writing. Marc Oliva, Fieldwork, geomorphological analysis and contribution to the revision of the manuscript. Manuel Rodríguez-Mena. Laboratory tasks (sample processing), processing of aerial photo imagery, geomorphological mapping and contribution to the writing. Irene Schimmelpfennig. Supervision of the whole laboratory sample processing, interpretation of the results and revision of the manuscript. Skafti Brynjólfsson Fieldwork, geomorphological analysis and contribution to the revision of the manuscript. þorsteinn Sæmundsson. Fieldwork, geomorphological analysis and contribution to the revision of the manuscript. José Juan Zamorano. Fieldwork, geomorphological analysis and mapping and contribution to the writing. José Úbeda. Geomorphological analysis and contribution to the revision of the manuscript. ASTER Team. AMS measurements of the 36Cl samples.

Appendix A. Supplementary data

Supplementary data to this article can be found online at https://doi.org/10.1016/j.quascirev.2021.107248.

References

Amschwand, D., Ivy-Ochs, S., Frehner, M., Steinemann, O., Christl, M., Vockenhuber, C., 2021. Deciphering the evolution of the Bleis Marscha rock glacier (Val d'Err, eastern Switzerland) with cosmogenic nuclide exposure dating, aerial image correlation, and finite-element modelling. Cryosphere Discuss. 1–40. https://doi.org/10.5194/tc-2020-209.

Andersen, C., Koç, N., Moros, M., 2004. A highly unstable Holocene climate in the subpolar North Atlantic: evidence from diatoms. Quat. Sci. Rev. 23, 2155–2166. https://doi.org/10.1016/j.quascirev.2018.04.024.

Anderson, L.S., Anderson, R.S., 2016. Modeling debris-covered glaciers: response to steady debris deposition. Cryosphere 10, 1105–1124. https://doi.org/10.5194/tc-10-1105-2016.

Anderson, R.S., Anderson, L.S., Armstrong, W.H., Rossi, M.W., Crump, S.E., 2018. Glaciation of alpine valleys: the glacier–debris-covered glacier–rock glacier continuum. Geomorphology 311, 127–142. https://doi.org/10.1016/j.geomorph.2018.03.015.

Andrés, N., Tanarro, L.M., Fernández, J.M., Palacios, D., 2016. The origin of glacial alpine landscape in Tröllaskagi Peninsula (North Iceland). Cuadernos Invest. Geogr. 42, 341–368. https://doi.org/10.18172/cig.2935.

Andrés, N., Gómez-Ortiz, A., Fernández-Fernández, J.M., Tanarro, L.M., Salvador-Franch, F., Oliva, M., Palacios, D., 2019. Timing of deglaciation and rock glacier origin in the southeastern Pyrenees: a review and new data. Boreas 47, 1050–1071. https://doi.org/10.1111/bor.12324.

Aydin, A., 2009. The ISRM suggested methods for rock characterization, testing and monitoring: 2007-2014. Int. J. Rock Mech. Min. Sci. 46, 627–634. https://doi.org/10.1007/978-3-319-07713-0.

Azócar, G., Brenning, A., 2010. Hydrological and geomorphological significance of rock glaciers in the dry Andes, Chile (27°-33°S). Permafr. Periglac. Process. 21 (1), 42–53. https://doi.org/10.1002/ppp.669.

Bahr, D.B., Meier, M.F., Peckham, S.D., 1997. The physical basis of glacier volume-area scaling. J. Geophys. Res.: Solid Earth 102 (B9), 20355–20362. https://doi.org/10.1029/97JB01696.

Bahr, D.B., Pfeffer, W.T., Kaser, G., 2015. A review of volume-area scaling of glaciers. Rev. Geophys. 53 (1), 95–140. https://doi.org/10.1002/2014RG000470.

Balco, G., Stone, J., Lifton, N., Dunai, T., 2008. A complete and easily accessible means of calculating surface exposure ages or erosion rates from 10Be and 26Al measurements. Quat. Geochronol. 3, 174–195. https://10.1016/j.quageo.2007.12.001.

Ballantyne, C.K., 1989. The Loch Lomond readvance on the isle of Skye, Scotland: glacier reconstruction and palaeoclimatic implications. J. Quat. Sci. 4, 95–108.

Bamber, J.L., Westaway, R.M., Marzeion, B., Wouters, B., 2018. The land ice contribution to sea level during the satellite era. Environ. Res. Lett. 13 (6), 063008. https://doi.org/10.1088/1748-9326/aadb2c.

Berthling, I., 2011. Beyond confusion: rock glaciers as cryo-conditioned landforms. Geomorphology 131, 98–106. https://doi.org/10.1016/j.geomorph.2011.05.002.

Bhambri, R., Bolch, T., Chaujar, R.K., Kulshreshtha, S.C., 2011. Glacier changes in the Garhwal Himalaya, India, from 1968 to 2006 based on remote sensing. J. Glaciol. 57, 543–556. https://doi.org/10.3189/002214311796905604.

Björnsson, H., 1971. Bægisarjökull, North Iceland. Results of gla- ciological investigations 1967–68. Part I. Mass balance and general meteorology. Jokull 21, 111–118.

Brenning, A., 2005. Geomorphological, hydrological and climatic significance of rock glaciers in the Andes of Central Chile (33-35°S). Permafr. Periglac. Process. 16, 231–240. https://doi.org/10.1002/ppp.528.

Campos, N., Tanarro, L.M., Palacios, D., Zamorano, J.J., 2019. Slow dynamics in debris-covered and rock glaciers in Hofsdalur, Tröllaskagi Peninsula (northern Iceland). Geomorphology 342, 61–77. https://doi.org/10.1016/j.geomorph.2019.06.005.

Caseldine, C.J., 1985. The extent of some glaciers in northern Iceland during the Little ice age and the nature of recent deglaciation. Geogr. J. 151, 215–227. https://doi.org/10.2307/633535.

Caseldine, C.J., Stotter, J., 1993. Little Ice Age" glaciation of Tröllaskagi peninsula, northern Iceland: climatic implications for reconstructed equilibrium line altitudes (ELAs). Holocene 3, 357–366. https://doi.org/10.1177/095968369300300408.

Caseldine, C.J., Cullingford, R.A., 1981. Recent mapping of Gljúfurárjökull and Gljúfurárdalur. Jokull 31, 11–22.

Charton, J., Jomelli, V., Schimmelpfennig, I., Verfaillie, D., Favier, V., Mokadem, F., et al., 2020. A debris-covered glacier at Kerguelen (49° S, 69° E) over the past 15 000 years. Antarct. Sci. 1–13. https://doi.org/10.1017/S0954102020000541.

Charton, J., Verfaillie, D., Jomelli, V., Francou, B., ASTER Team, 2021. Early Holocene rock glacier stabilisation at col. du Lautaret (French Alps): palaeoclimatic implications. Geomorphology. https://doi.org/10.1016/j.geomorph.2021.107962.

Chenet, M., Roussel, E., Jomelli, V., Grancher, D., 2010. Asynchronous Little Ice Age glacial maximum extent in southeast Iceland. Geomorphology 114, 253–260. https://doi.org/10.1016/j.geomorph.2009.07.012.

Cossart, E., Mercier, D., Decaulne, A., Feuillet, T., Jónsson, H.P., Saemundsson, þ., 2014. Impacts of post-glacial rebound on landslide spatial distribution at a regional scale in northern Iceland (Skagafjörður). Earth Surf. Process. Landforms 39, 336–350. https://doi.org/10.1002/esp.3450.

Crump, S.E., Anderson, L.S., Miller, G.H., Anderson, R.S., 2017. Interpreting exposure ages from ice-cored moraines: a Neoglacial case study on Baffin Island, Arctic Canada. J. Quat. Sci. 32 (8), 1049–1062. https://doi.org/10.1002/jqs.2979.

Czekirda, J., Westermann, S., Etzelmüller, B., Jóhannesson, T., 2019. Transient modelling of permafrost distribution in Iceland. Front. Earth Sci. 7. https://doi.org/10.3389/feart.2019.00130. Article 130.

Dahl, S.O., Nesje, A., 1992. Paleoclimatic implications based on equilibrium-line altitude depressions of reconstructed Younger Dryas and Holocene cirque glaciers in inner Nordfjord, western Norway. Palaeogeogr. Palaeoclimatol. Palaeoecol. 94, 87–97.

Decaulne, A., Cossart, E., Mercier, D., Feuillet, T., Coquin, J., Jónsson, H.P., 2016. An early Holocene age for the Vatn landslide (Skagafjörður, central northern Iceland): insights into the role of postglacial landsliding on slope development. Holocene 26, 1304–1318. https://doi.org/10.1177/0959683616638432.

Deline, P., 2005. Change in surface debris cover on Mont Blanc massif glaciers after the ‘Little Ice Age’ termination. Holocene 15, 302–309. https://doi.org/10.1016/j.gloplacha.2009.05.003.

Deline, P., Akçar, N., Ivy-Ochs, S., Kubik, P.W., 2015. Repeated Holocene rock avalanches onto the Brenva Glacier, Mont Blanc massif, Italy: a chronology. Quat. Sci. Rev. 126, 186–200. https://doi.org/10.1016/j.quascirev.2015.09.004.

Emmer, A., Loarte, E.C., Klimeš, J., Vilímek, V., 2015. Recent evolution and degradation of the bent Jatunraju glacier (Cordillera Blanca, Peru). Geomorphology 228, 345–355. https://doi.org/10.1016/J.GEOMORPH.2014.09.018.

Eriksen, H.Ø., Rouyet, L., Lauknes, T.R., Berthling, I., Isaksen, K., Hindberg, H., Corner, G.D., 2018. Recent acceleration of a rock glacier complex, Ádjet, Norway, documented by 62 Years of remote sensing observations. Geophys. Res. Lett. 45 (16), 8314–8323. https://doi.org/10.1029/2018GL077605.

Etzelmüller, B., Farbrot, H., Guðmundsson, Á., Humlum, O., Tveito, O.E., Björnsson, H., 2007. The regional distribution of mountain permafrost in Iceland. Permafr. Periglac. Process. 18, 185–199. https://doi.org/10.1002/ppp.583.

Etzelmüller, B., Patton, H., Schomacker, A., Czekirda, J., Girod, L., Hubbard, A., Lilleøren, K.S., Westermann, S., 2020. Icelandic permafrost dynamics since the Last Glacial Maximum - model results and geomorphological implications. Quat. Sci. Rev. 233, 106236. https://doi.org/10.1016/j.quascirev.2020.106236.

Evans, D.J.A., Archer, S., Wilson, D.J.H., 1999. A comparison of the lichenometric and Schmidt hammer dating techniques based on data from the proglacial areas of

some Icelandic glaciers. Quat. Sci. Rev. 18 (1), 13–41.
Ewertowski, M.W., Evans, D.J.A., Roberts, D.H., Tomczyk, A.M., Ewertowski, W., Pleksot, K., 2019. Quantification of historical landscape change on the foreland of a receding polythermal glacier, Hørbyebreen, Svalbard. Geomorphology 325, 40–54. https://doi.org/10.1016/j.geomorph.2018.09.027.
Ferguson, J., Vieli, A., 2020. Modelling steady states and the transient response of debris-covered glaciers. Cryosphere Discuss. 1–31. https://doi.org/10.5194/tc-2020-228.
Fernández-Fernández, J.M., Andrés, N., Sæmundsson, Þ., Brynjólfsson, S., Palacios, D., 2017. High sensitivity of North Iceland (Tröllaskagi) debris-free glaciers to climatic change from the "Little Ice Age" to the present. Holocene 27, 1–14. https://doi.org/10.1177/0959683616683262.
Fernández-Fernández, J.M., Andrés de Pablo, N., 2018. Methodological proposal for the analysis of the evolution of glaciers since the Little Ice Age and its application in the Tröllaskagi Peninsula (Northern Iceland). Cuadernos de investigación geográfica/Geographical Research Letters, pp. 69–97. https://doi.org/10.18172/cig.3392.
Fernández-Fernández, J.M., Palacios, D., Andrés, N., Schimmelpfennig, I., Brynjólfsson, S., Sancho, L.G., Zamorano, J.J., Heiðmarsson, S., Sæmundsson, Þ., ASTER Team, 2019. A multi-proxy approach to Late Holocene fluctuations of Tungnahryggsjökull glaciers in the Tröllaskagi peninsula (northern Iceland). Sci. Total Environ. 664, 499–517. https://doi.org/10.1016/j.scitotenv.2019.01.364.
Fernández-Fernández, J.M., Palacios, D., Andrés, N., Schimmelpfennig, I., Tanarro, L.M., López-Acevedo, F.J., Sæmundsson, Þ., Team, A.S.T.E.R., 2020. Constraints on the timing of debris-covered and rock glaciers: an exploratory case study in the Hólar area, northern Iceland. Geomorphology 361, 107196. https://doi.org/10.1016/j.geomorph.2020.107196.
Fink, D., Vogt, S., Hotchkis, M., 2000. Cross-sections for 36Cl from Ti at Ep=35–150 MeV: applications to in-situ exposure dating. Nucl. Instrum. Methods Phys. Res. Sect. B Beam Interact. Mater. Atoms 172, 861–866. https://doi.org/10.1016/S0168-583X(00)00200-7.
Gardner, A.S., Moholdt, G., Cogley, J.G., Wouters, B., Arendt, A.A., Wahr, J., Berthier, E., Hock, R., Pfeffer, W.T., Kaser, G., Ligtenberg, S.R., Bolch, T., Sharp, M.J., Hagen, J.O., Ove, J., van den Broeke, M.R., Paul, P., 2013. A reconciled estimate of glacier contributions to sea level rise: 2003 to 2009. Science 340 (6134), 852–857. https://doi.org/10.1126/science.1234532.
Geirsdóttir, Á., Miller, G.H., Andrews, J.T., Harning, D.J., Anderson, L.S., Florian, C., Larseb, D., Thordarson, T., 2019. The onset of Neoglaciation in Iceland and the 4.2 ka event. Clim. Past 15, 25–40. https://doi.org/10.5194/cp-15-25-2019.
Geirsdóttir, Á., Miller, G.H., Andrews, J.T., Harning, D.J., Anderson, L.S., Thordarson, T., 2018. The onset of Neoglaciation in Iceland and the 4.2 ka event. Clim. Past Discuss. 1–33. https://doi.org/10.5194/cp-2018-130.
Geirsdóttir, Á., Miller, G.H., Axford, Y., Ólafsdóttir, Sædís, 2009. Holocene and latest Pleistocene climate and glacier fluctuations in Iceland. Quat. Sci. Rev. 28, 2107–2118. https://doi.org/10.1016/j.quascirev.2009.03.013.
Geirsdóttir, Á., Miller, G.H., Larsen, D.J., Ólafsdóttir, S., 2013. Abrupt Holocene climate transitions in the northern North Atlantic region recorded by synchronized lacustrine records in Iceland. Quat. Sci. Rev. 70, 48–62. https://doi.org/10.1016/j.quascirev.2013.03.010.
Gibson, M.J., Glasser, N.F., Quincey, D.J., Rowan, A.V., Irvine-Fynn, T.D., 2017. Changes in glacier surface cover on Baltoro glacier, Karakoram, north Pakistan, 2001–2012. J. Maps 13, 100–108. https://doi.org/10.1080/17445647.2016.1264319.
Glasser, N.F., Holt, T.O., Evans, Z.D., Davies, B.J., Pelto, M., Harrison, S., 2016. Recent spatial and temporal variations in debris cover on Patagonian glaciers. Geomorphology 273, 202–216. https://doi.org/10.1016/j.geomorph.2016.07.036.
Häberle, T., 1991. Holocene glacial history of the Hörgádalur area, Tröllaskagi, northern Iceland. In: En, Maizels, J.K., Caseldine, C. (Eds.), Environmental Change in Iceland: Past and Present. Kluwer Academic Publishers, Dordrecht, pp. 193–202. https://doi.org/10.1007/978-94-011-3150-6_13.
Hambrey, M.J., Quincey, D.J., Glasser, N.F., Reynolds, J.M., Richardson, S.J., Clemmens, S., 2008. Sedimentological, geomorphological and dynamic context of debris-mantled glaciers, Mount Everest (Sagarmatha) region, Nepal. Quat. Sci. Rev. 27, 2361–2389. https://doi.org/10.1016/j.quascirev.2008.08.010.
Hannesdóttir, H., Sigurðsson, O., Þrastarson, R. H., Guðmundsson, S., Belart, J. M., Pálsson, F., et al. A national glacier inventory and variations in glacier extent in Iceland from the Little Ice Age maximum to 2019. Jokull, 50, 1-34. doi: 10.33799/jokull2020.70.001.
Herreid, S., Pellicciotti, F., 2020. The state of rock debris covering Earth's glaciers. Nat. Geosci. 13 (9), 621–627. https://doi.org/10.1038/s41561-020-0615-0.
Humlum, O., 2000. The geomorphic significance of rock glaciers: estimates of rock glacier debris volumes and headwall recession rates in West Greenland. Geomorphology 35, 41–67. https://doi.org/10.1016/S0169-555X(00)00022-2.
Janke, J.R., 2005. Photogrammetric analysis of front range rock glacier flow rates. Geogr. Ann. Phys. Geogr. 87, 515–526. https://doi.org/10.1111/j.0435-3676.2005.00275.x.
Janke, J.R., Bellisario, A.C., Ferrando, F.A., 2015. Classification of debris-covered glaciers and rock glaciers in the Andes of central Chile. Geomorphology 241, 98–121. https://doi.org/10.1016/j.geomorph.2015.03.034.
Janke, J.R., Regmi, N.R., Giardino, J.R., Vitek, J.D., 2013. Rock glaciers. In: Shroder, J., Giardino, R., Harbor, J. (Eds.), Treatise on Geomorphology, Glacial and Periglacial Geomorphology, vol. 8. Academic Press, San Diego, CA, pp. 238–273. https://doi.org/10.1016/B978-0-12-374739-6.00211-6.
Jones, D.B., Harrison, S., Anderson, K., 2019. Mountain glacier-to-rock glacier transition. Global Planet. Change 181, 102999. https://doi.org/10.1016/j.gloplacha.2019.102999.
Jónsson, O., 1976. Berghlaup. Ræktunarfélag Norðurlands, Akureyri.
Kääb, A., Jacquemart, M., Gilbert, A., Leinss, S., Girod, L., Huggel, C., et al., 2021. Sudden large-volume detachments of low-angle mountain glaciers–more frequent than thought. Cryosphere Discuss. 1–52. https://doi.org/10.5194/tc-2020-243.
Kellerer-Pirklbauer, A., Lieb, G.K., Kaufmann, V., 2017. The Dösen Rock Glacier in Central Austria: a key site for multidisciplinary long-term rock glacier monitoring in the Eastern Alps. Aust. J. Earth Sci. 110. https://doi.org/10.17738/ajes.2017.0013.
Kellerer-Pirklbauer, A., Wangensteen, B., Farbrot, H., Etzelmüller, B., 2007. Relative surface age-dating of rock glacier systems near Hólar in Hjaltadalur, northern Iceland. J. Quat. Sci. 23, 137–151. https://doi.org/10.1002/jqs.1117.
Kenner, R., 2019. Geomorphological analysis on the interaction of Alpine glaciers and rock glaciers since the Little Ice Age. Land Degrad. Dev. 30 (5), 580–591. https://doi.org/10.1002/ldr.3238.
Kirkbride, M.P., 2000. Ice-marginal geomorphology and Holocene expansion of debris-covered Tasman glacier, New Zealand. In: Nakawo, M., Raymond, C.F., Fountain, A. (Eds.), Debris-covered Glaciers, vol. 264. IAHS, pp. 211–217. http://hydrologie.org/redbooks/a264/iahs_264_0211.pdf.
Kirkbride, M.P., 2011. Debris-covered glaciers. In: Singh, V.P., Singh, P., Haritashya, U.K. (Eds.), Encyclopedia of Snow, Ice and Glaciers: Encyclopedia of Earth Series. Springer, Netherlands, pp. 180–182. https://doi.org/10.1007/978-90-481-2642-2_622.
Kirkbride, M.P., Dugmore, A.J., 2006. Responses of mountain ice caps in central Iceland to Holocene climate change. Quat. Sci. Rev. 25, 1692–1707. https://doi.org/10.1016/j.quascirev.2005.12.004.
Kirkbride, M.P., Dugmore, A.J., 2008. Two millennia of glacier advances from southern Iceland dated by tephrochronology. Quat. Res. 70, 398–411. https://doi.org/10.1016/j.yqres.2008.07.001.
Knight, J., Harrison, S., Jones, D.B., 2019. Rock glaciers and the geomorphological evolution of deglacierizing mountains. Geomorphology 324, 14–24. https://doi.org/10.1016/j.geomorph.2018.09.020.
Koblet, T., Gärtner-Roer, I., Zemp, M., Jansson, P., Thee, P., Haeberli, W., Holmlund, P., 2010. Reanalysis of multi-temporal aerial images of Storglaciären, Sweden (1959-99); Part 1: determination of length, area, and volume changes. Cryosphere 4, 333–343. https://doi.org/10.5194/tc-4-333-2010.
Kugelmann, O., 1991. Dating recent glacier advances in the Svarfadardalur-Skíðadalur area of northern Iceland by means of a new lichen curve. In: Maizels, J.K., Caseldine, C. (Eds.), Environmental Change in Iceland: Past and Present, Glaciology and Quaternary Geology, vol. 7. Springer, Dordrecht, pp. 203–217. https://doi.org/10.1007/978-94-011-3150-6_14.
Lal, D., 1991. Cosmic ray labeling of erosion surfaces: in situ nuclide production rates and erosion models. Earth Planet Sci. Lett. 104, 424–439. https://doi.org/10.1016/0012-821X(91)90220-C.
Lambiel, C., Maillard, B., Regamei, B., Martin, S., Kummert, M., Schoeneich, P., Reynard, E., 2013. Adaptation of the geomorphological mapping system of the university of Lausanne for ArcGIS. et al.. In: 8th International Conference on Geomorphology (IAG) Abstract, p. 1176 (Paris).
Lambrecht, A., Mayer, C., Hagg, W., Popovnin, V., Rezepkin, A., Lomidze, N., Svanadze, D., 2011. A comparison of glacier melt on debris-covered glaciers in the northern and southern Caucasus. Cryosphere 5, 525–538. https://doi.org/10.1016/j.gloplacha.2009.05.003.
Larsen, D.J., Miller, G.H., Geirsdóttir, Á., Ólafsdóttir, S., 2012. Non-linear Holocene climate evolution in the North Atlantic: a high-resolution, multi-proxy record of glacier activity and environmental change from Hvítárvatn, central Iceland. Quat. Sci. Rev. 39, 14–25. https://doi.org/10.1016/j.quascirev.2012.02.006.
Larsen, D.J., Miller, G.H., Geirsdóttir, Á., Thordarson, T., 2011. A 3000-year varved record of glacier activity and climate change from the proglacial lake Hvítárvatn, Iceland. Quat. Sci. Rev. 30, 2715–2731. https://doi.org/10.1016/j.quascirev.2011.05.026.
Li, Y.K., 2018. Determining topographic shielding from digital elevation models for cosmogenic nuclide analysis: a GIS model for discrete sample sites. J. Mt. Sci. 15 (5), 939–947. https://doi.org/10.1007/s11629-018-4895-4.
Licciardi, J.M., Denoncourt, C.L., Finkel, R.C., 2008. Cosmogenic 36Cl production rates from Ca spallation in Iceland. Earth Planet Sci. Lett. 267, 365–377. https://doi.org/10.1016/j.epsl.2007.11.036.
Lilleøren, K.S., Etzelmüller, B., Gärtner-Roer, I., Kääb, A., Westermann, S., Gumundsson, Á., 2013. The distribution, thermal characteristics and dynamics of permafrost in Tröllaskagi, Northern Iceland, as inferred from the distribution of rock glaciers and ice-cored moraines. Permafr. Periglac. Process. 24 (4), 322–335. https://doi.org/10.1002/ppp.1792.
Linge, H., Nesje, A., Matthews, J.A., Fabel, D., Xu, S., 2020. Evidence for rapid paraglacial formation of rock glaciers in southern Norway from 10Be surface-exposure dating. Quat. Res. 1–16. https://doi.org/10.1017/qua.2020.10.
Longhi, A., Guglielmin, M., 2020. Reconstruction of the glacial history after the Last Glacial Maximum in the Italian Central Alps using Schmidt's hammer R-values and crystallinity ratio indices of soils. Quat. Int. 558, 19–27. https://doi.org/10.1016/j.quaint.2020.08.045.
Mackay, S.L., Marchant, D.R., 2016. Dating buried glacier ice using cosmogenic 3He in surface clasts: theory and application to Mullins Glacier, Antarctica. Quat. Sci. Rev. 140, 75–100. https://doi.org/10.1016/j.quascirev.2016.03.013.
Maizels, J.K., Dugmore, A.J., 1985. Lichenometric dating and tephrochronology of sandur deposits, Sólheimajökull area, southern Iceland. Jokull (35), 69–78.
Marr, P., Winkler, S., Löffler, J., 2019. Schmidt-hammer exposure-age dating (SHD)

performed on periglacial and related landforms in Opplendskedalen, Geirangerfjellet, Norway: implications for mid-and late-Holocene climate variability. Holocene 29 (1), 97–109. https://doi.org/10.1177/0959683618804634.
Marrero, S.M., Phillips, F.M., Caffee, M.W., Gosse, J.C., 2016. Cronus - earth cosmogenic 36Cl calibration. Quat. Geochronol. 31, 199–219. https://doi.org/10.1016/j.quageo.2015.10.002.
Martin, L., Blard, P.-H., Balco, G., Lave, J., Delunel, R., Lifton, N., Laurent, V., 2017. The CREp program and the ICE-D production rate calibration database: a fully parameterizable and updated online tool to compute cosmic-ray exposure ages. Quat. Geochronol. 38, 25–49. https://doi.org/10.1016/j.quageo.2016.11.006.
Matthews, J.A., Nesje, A., Linge, H., 2013. Relict talus-foot rock glaciers at Øyberget, Upper Ottadalen, Southern Norway: Schmidt hammer exposure ages and palaeoenvironmental implications. Permafr. Periglac. Process. 24 (4), 336–346. https://doi.org/10.1002/ppp.1794.
Matthews, J.A., Owen, G., 2010. Schmidt hammer exposure-age dating: developing linear age-calibration curves using Holocene bedrock surfaces from the Jotunheimen–Jostedalsbreen regions of southern Norway. Boreas 39 (1), 105–115. https://doi.org/10.1111/j.1502-3885.2009.00107.x.
Matthews, J.A., Winkler, S., 2011. Schmidt-hammer exposure-age dating (SHD): application to early Holocene moraines and a reappraisal of the reliability of terrestrial cosmogenic-nuclide dating (TCND) at Austanbotnbreen, Jotunheimen, Norway. Boreas 40 (2), 256–270. https://doi.org/10.1111/j.1502-885.2010.00178.x.
Mayr, E., Hagg, W., 2019. Debris-covered glaciers. In: Heckmann, T., Morche, D. (Eds.), Geomorphology of Proglacial Systems. Geography of the Physical Environment, pp. 59–71. https://doi.org/10.1007/978-3-319-94184-4_4.
Meier, M.F., Post, A.S., 1962. Recent Variations in Mass Net Budgets of Glaciers in Western North America, vol. 58. International Association of Hydrological Sciences Publication, pp. 63–77.
Merchel, S., Bremser, W., Alfimov, V., Arnold, M., Aumaître, G., Benedetti, L., Bourlès, D.L., Caffee, M., Fifield, L.K., Finkel, R.C., Freeman, S.P.H.T., Martschini, M., Matsushi, Y., Rood, D.H., Sasa, K., Steier, P., Takahashi, T., Tamari, M., Tims, S.G., Tosaki, Y., Wilcken, K.M., Xu, S., 2011. Ultra-trace analysis of 36Cl by accelerator mass spectrometry: an interlaboratory study. Anal. Bioanal. Chem. 400, 3125–3132. https://doi.org/10.1007/s00216-011-4979-2.
Mercier, D., Cossart, E., Decaulne, A., Feuillet, T., Jónsson, H.P., Sæmundsson, Þ., 2013. The Höfðahólar rock avalanche (sturzström): chronological constraint of paraglacial landsliding on an Icelandic hillslope. Holocene 23, 432–446. https://doi.org/10.1177/0959683612463104.
Mertes, J.R., Gulley, J.D., Benn, D.I., Thompson, S.S., Nicholson, L.I., 2017. Using structure-from-motion to create glacier DEMs and orthoimagery from historical terrestrial and oblique aerial imagery. Earth Surf. Process. Landforms 42, 2350–2364. https://doi.org/10.1002/esp.4188.
Midgley, N.G., Tonkin, T.N., 2017. Reconstruction of former glacier surface topography from archive oblique aerial images. Geomorphology 282, 18–26. https://doi.org/10.1016/j.geomorph.2017.01.008.
Miller, G.H., Brigham-Grette, J., Alley, R.B., Anderson, L., Bauch, H.A., Douglas, M.S.V., Edwards, M.E., Elias, S.A., Finney, B.P., Fitzpatrick, J.J., Funder, S.V., Herbert, T.D., Hinzman, L.D., Kaufman, D.S., MacDonald, G.M., Polyak, L., Robock, A., Serreze, M.C., Smol, J.P., Spielhagen, R., White, J.W.C., Wolfe, A.P., Wolff, E.W., 2010. Temperature and precipitation history of the Arctic. Quat. Sci. Rev. 29, 1679–1715. https://doi.org/10.1016/j.quascirev.2010.03.001.
Mölg, N., Bolch, T., 2017. Structure-from-Motion using historical aerial images to analyse changes in glacier surface elevation. Rem. Sens. 2017 (9), 1021. https://doi.org/10.3390/rs9101021.
Monnier, S., Kinnard, C., 2015. Reconsidering the glacier to rock glacier transformation problem: new insights from the central Andes of Chile. Geomorphology 238, 47–55. https://doi.org/10.1016/j.geomorph.2015.02.025.
Monnier, S., Kinnard, C., 2016. Pluri-decadal (1955–2014) evolution of glacier–rock glacier transitional landforms in the central Andes of Chile (30–33° S). Earth Surf. Dynam. 5, 493–509. https://doi.org/10.5194/esurf-5-493-2017.
Moore, A.K., Granger, D.E., 2019. Calibration of the production rate of cosmogenic 36Cl from Fe. Quat. Geochronol. 51, 87–98. https://doi.org/10.1016/j.quageo.2019.02.002.
Morino, C., Conway, S.J., Sæmundsson, Þ., Kristinsson, J.H., Hillier, Butcher, F., Balme, M.R., Colm, J., Argles, T., 2019. Molards as a marker of permafrost degradation and landslide processes. Earth Planet Sci. Lett. 516, 136–147. https://doi.org/10.1016/j.epsl.2019.03.040.
Muscheler, R., Beer, J., Kubik, P.W., Synal, H.A., 2005. Geomagnetic field intensity during the last 60,000 years based on 10Be and 36Cl from the Summit ice cores and 14C. Quat. Sci. Rev. 24 (16–17), 1849–1860. https://doi.org/10.1016/j.quascirev.2005.01.012.
Niedzielski, T., Migon, P., Placek, A., 2009. A minimum sample size required from Schmidt hammer measurements Earth. Surf. Process. Landforms 34, 1713–1725. https://doi.org/10.1002/esp, 2009.
NOAA, 1976. (National Oceanic and Atmospheric Administration) U.S. Standard Atmosphere. US Gov. Print. Off. https://www.ngdc.noaa.gov/stp/space-weather/online-publications/miscellaneous/us-standard-atmosphere-1976/us-standard-atmosphere_st76-1562_noaa.pdf.
Nývlt, D., Braucher, R., Engel, Z., Mlčoch, B., 2014. Timing of the northern prince Gustav ice stream retreat and the deglaciation of northern james Ross island, Antarctic peninsula during the last glacial-interglacial transition. Quat. Res. 82, 441–449. https://doi.org/10.1016/j.yqres.2014.05.003.
Ogilvie, A.E., Jónsson, T., 2001. Little ice age" research: a perspective from Iceland. Climatic Change 48 (1), 9–52. https://doi.org/10.1023/A:1005625729889.
Osmaston, H., 2005. Estimates of glacier equilibrium line altitudes by the area × altitude, the area × altitude balance ratio and the area × altitude balance index methods and their validation. Quat. Int. 138–139, 22–31. https://doi.org/10.1016/j.quaint.2005.02.004.
Otto, J.C., Dikau, R., 2004. Geomorphic system analysis of a high mountain valley in the Swiss Alps. Zeitschrift für Geomorphol. N.F. 48 (3), 323–341.
Palacios, D., Rodríguez-Mena, M., Fernández-Fernández, J.M., Schimmelpfennig, I., Tanarro, L.M., Zamorano, J.J., Andrés, N., Úbeda, J., Sæmundsson, Þ., Brynjólfsson, S., Oliva, M., ASTER Team, 2021. Reversible glacial-periglacial transition in response to climate changes and paraglacial dynamics: a case study from Héðinsdalsjökull (northern Iceland). Geomorphology 388, 107787. https://doi.org/10.1016/j.geomorph.2021.107787.
Pellitero, R., Rea, B.R., Spagnolo, M., Bakke, J., Hughes, P., Ivy-Ochs, S., Lukas, S., Ribolini, A., 2015. A GIS tool for automatic calculation of glacier equilibrium-line altitudes. Comput. Geosci. 82, 55–62. https://doi.org/10.1016/j.cageo.2015.05.005.
Pellitero, R., Rea, B.R., Spagnolo, M., Bakke, J., Ivy-Ochs, S., Frew, C.R., Hughes, P., Ribolini, A., Lukas, S., Renssen, H., 2016. GlaRe, a GIS tool to reconstruct the 3D surface of palaeoglaciers. Comput. Geosci. 94, 77–85. https://doi.org/10.1016/j.cageo.2016.06.008.
Pétursson, H.G., Norðdahl, H., Ingólfsson, O., 2015. Late Weischelian history of relative sea level changes in Iceland during a collapse and subsequent retreat of marine based ice sheet. Cuadernos Invest. Geogr. 41, 261–277. https://doi.org/10.18172/cig.2741.
Piermattei, L., Carturan, L., Guarnieri, A., 2015. Use of terrestrial photogrammetry based on structure-from-motion for mass balance estimation of a small glacier in the Italian alps. Earth Surf. Process. Landforms 40 (13), 1791–1802. https://doi.org/10.1002/esp.3756.
Piermattei, L., Carturan, L., de Blasi, F., Tarolli, P., Dalla Fontana, G., Vettore, A., Pfeifer, N., 2016. Suitability of ground-based SfM–MVS for monitoring glacial and periglacial processes. Earth Surf. Dynam. 4, 425–443. https://doi.org/10.5194/esurf-4-425-2016.
Porter, S.C., 1975. Equilibrium-line altitudes of late quaternary glaciers in the southern alps, New Zealand. Quat. Res. 5 (1), 27–47. https://doi.org/10.1016/0033-5894(75)90047-2.
Potter, N.J., Steig, E.J., Clark, D.H., Speece, M.A., Clark, G.M., Updike, A.B., 1998. Galena Creek rock glacier revisited—new observations on an old controversy. Geogr. Ann. Phys. Geogr. 80, 251–265. https://doi.org/10.1111/j.0435-3676.1998.00041.x.
Quincey, D.J., Glasser, N.F., 2009. Morphological and ice-dynamical changes on the Tasman glacier, New Zealand, 1990–2007. Glob. Planet. Change 68 185–197.
Tielidze, L.G., Bolch, T., Wheate, R.D., Kutuzov, S.S., Lavrentiev, I.I., Zemp, M., 2020a. Supra-glacial debris cover changes in the Greater Caucasus from 1986 to 2014. Cryosphere 14, 585–598. https://doi.org/10.5194/tc-14-585-2020.
Renssen, H., Seppä, H., Crosta, X., Goosse, H., Roche, D.M., 2012. Global characterization of the holocene thermal maximum. Quat. Sci. Rev. 48, 7–19.
Rode, M., Kellerer-Pirklbauer, A., 2012. Schmidt-hammer exposure-age dating (SHD) of rock glaciers in the Schöderkogel-Eisenhut area, Schladminger Tauern Range, Austria. Holocene 22 (7), 761–771. https://doi.org/10.1177/0959683611430410.
Roe, G.H., Baker, M.B., Herla, F., 2017. Centennial glacier retreat as categorical evidence of regional climate change. Nat. Geosci. 10 (2), 95–99. https://doi.org/10.1038/ngeo2863.
Rodríguez-Mena, M., Fernández-Fernández, J.M., Tanarro, L.M., Zamorano, J.J., Palacios, D., 2021. Héðinsdalsjökull, northern Iceland: geomorphology recording the recent complex evolution of a glacier. J. Maps 17 (2), 301–313. https://doi.org/10.1080/17445647.2021.1920056.
Rowan, A.V., Egholm, D.L., Quincey, D.J., Glasser, N.F., 2015. Modelling the feedbacks between mass balance, ice flow and debris transport to predict the response to climate change of debris-covered glaciers in the Himalaya. Earth Planet Sci. Lett. 430, 427–438. https://doi.org/10.1016/j.epsl.2015.09.004.
Rundgren, M., 1995. Biostratigraphic evidence of the Allerød -younger dryas-preboreal oscillation in northern Iceland. Quat. Res. 44, 405–416.
Rundgren, M., 1999. A summary of the environmental history of the Skagi peninsula, northern Iceland, 11,300-7800 BP. Jokull 47, 1–19.
Sæmundsson, K., Kristjansson, L., McDougall, I., Watkins, N.D., 1980. K-Ar dating, geological and paleomagnetic study of a 5-km lava succession in northern Iceland. J. Geophys. Res.: Solid Earth 85, 3628–3646. https://doi.org/10.1029/JB085iB07p03628.
Sæmundsson, Þ., Morino, C., Helgason, J.K., Conway, S.J., Pétursson, H.G., 2018. The triggering factors of the Móafellshyrna debris slide in northern Iceland: intense precipitation, earthquake activity and thawing of mountain permafrost. Sci. Total Environ. 621, 1163–1175. https://doi.org/10.1016/J.SCITOTENV.2017.10.111.
Scherler, D., Egholm, D.L., 2020. Production and transport of supraglacial debris: insights from cosmogenic 10Be and numerical modeling, Chhota Shigri Glacier, Indian Himalaya. J. Geophys. Res.: Earth Surface 125 (10), e2020JF005586. https://doi.org/10.1029/2020JF005586.
Schimmelpfennig, I., Benedetti, L., Garreta, V., Pik, R., Blard, P.H., Burnard, P., Bourlès, D., Finkel, R., Ammon, K., Dunai, T., 2011. Calibration of cosmogenic 36Cl production rates from Ca and K spallation in lava flows from Mt. Etna (38°N, Italy) and Payun Matru (36°S, Argentina). Geochem. Cosmochim. Acta 75, 2611–2632. https://doi.org/10.1016/j.gca.2011.02.013.
Schimmelpfennig, I., Schaefer, J.M., Putnam, A.E., Koffman, T., Benedetti, L., Ivy-Ochs, S., Team, A., Schlüchter, C., 2014. 36Cl production rate from K-spallation in the European Alps (Chironico landslide, Switzerland). J. Quat. Sci. 29, 407–413.

https://doi.org/10.1002/jqs.2720.
Schimmelpfennig, I., Tesson, J., Blard, P.H., Benedetti, L., Zakari, M., Balco, G., 2019. The CREp Chlorine-36 Exposure Age and Depth Profile Calculator. Goldschmidt. Spain, Barcelona. https://goldschmidtabstracts.info/2019/2996.pdf.
Shukla, A., Gupta, R.P., Arora, M.K., 2009. Estimation of debris cover and its temporal variation using optical satellite sensor data: a case study in Chenab basin, Himalaya. J. Glaciol. 55 (191), 444–452. https://doi.org/10.3189/002214309788816632.
Shukla, T., Mehta, M., Kumar, V., Nainwal, H.C., Dobhal, D.P., 2017. Application of the Schmidt-hammer with relative-age dating of moraine boulders—a case study from Mandakini River valley, central Himalaya, India. Himal. Geol. 38 (2), 184–192.
Sigurðsson, O., Williams, R.S., National Energy Authority Island, 2008. Geographic Names of Iceland's Glaciers: Historic and Modern. US Geological Survey., Reston, VA. ISBN 0-607-97815-9.
Sissons, J.B., 1974. A late glacial ice cap in the central grampians, Scotland. Trans. Inst. Br. Geogr. 62, 95–114.
Spreafico, M.C., Sternai, P., Agliardi, F., 2021. Paraglacial rock-slope deformations: sudden or delayed response? Insights from an integrated numerical modelling approach. Landslides 18, 1311–1326. https://doi.org/10.1007/s10346-020-01560-x.
Stone, J.O., 2000. Air pressure and cosmogenic isotope production. J. Geophys. Res. 105, 23753–23759. https://doi.org/10.1029/2000JB900181/2000.
Storni, E., Hugentobler, M., Manconi, A., Loew, S., 2020. Monitoring and analysis of active rockslide-glacier interactions (Moosfluh, Switzerland). Geomorphology 371, 107414. https://doi.org/10.1016/j.geomorph.2020.107414.
Stötter, J., 1990. Geomorphologische und landschaftsgeschichtliche Untersuchungen im Svarfaðardalur-Skiðadalur, Tröllaskagi, N-Island. Munch. Geogr. Abhand. 9, 1–166.
Stötter, J., Wastl, M., Caseldine, C., Häberle, T., 1999. Holocene palaeoclimatic reconstruction in northern Iceland: approaches and results. Quat. Sci. Rev. 18, 457–474. https://doi.org/10.1016/S0277-3791(98)00029-8.
Striberger, J., Björck, S., Holmgren, S., Hamerlík, L., 2012. Th sediments of Lake Lögurinn—A unique proxy record of Holocene glacial meltwater variability in eastern Iceland. Quat. Sci. Rev. 38, 76–88. https://doi.org/10.1016/j.quascirev.2012.02.001.
Striberger, J., Björck, S., Benediktsson, Í.Ö., Snowball, I., Uvo, C.B., Ingólfsson, Ó., Kjær, K.H., 2011. Climatic control of the surge periodicity of an Icelandic outlet glacier. J. Quat. Sci. 26 (6), 561–565. https://doi.org/10.1002/jqs.1527.
Sumner, P., Nel, W., 2002. The effect of rock moisture on Schmidt hammer rebound: tests on rock samples from Marion Island and South Africa. Earth Surf. Process. Landforms 27 (10), 1137–1142. https://doi.org/10.1002/esp.402.
Tanarro, L.M., Palacios, D., Zamorano, J.J., Andrés, N., 2018. Proposal for geomorphological mapping of debris-covered and rock glaciers and its application to Tröllaskagi Peninsula (Northern Iceland). J. Maps 14, 692–703. https://doi.org/10.1080/17445647.2018.1539417.
Tanarro, L.M., Fernández, J.M., Andres, N., Zamorano, J.J., Sæmundsson, Þ., Brynjólfsson, S., Palacios, D., 2019. Unchanged surface morphology of debris-covered glacier and rock glaciers in Tröllaskagi Peninsula (Northern Iceland). Sci. Total Environ. 648, 218–235. https://doi.org/10.1016/j.scitotenv.2018.07.460.
Thakuri, S., Salerno, F., Smiraglia, C., Bolch, T., D'Agata, C., Viviano, G., Tartari, G., 2014. Tracing glacier changes since the 1960s on the south slope of Mt. Everest (central Southern Himalaya) using optical satellite imagery. https://doi.org/10.5194/tc-8-1297-2014.
Tielidze, L.G., Bolch, T., Wheate, R.D., Kutuzov, S.S., Lavrentiev, I.I., Zemp, M., 2020b. Supra-glacial debris cover changes in the Greater Caucasus from 1986 to 2014. Cryosphere 14, 585–598. https://doi.org/10.5194/tc-14-585-2020.
Tomkins, M.D., Dortch, J.M., Hughes, P.D., 2016. Schmidt Hammer exposure dating (SHED): establishment and implications for the retreat of the last British Ice Sheet. Quat. Geochronol. 33, 46–60. https://doi.org/10.1016/j.quageo.2016.02.002.
Tomkins, M.D., Dortch, J.M., Hughes, P.D., Huck, J.J., Stimson, A.G., Delmas, M., et al., 2018a. a. Rapid age assessment of glacial landforms in the Pyrenees using Schmidt hammer exposure dating (SHED). Quat. Res. 90 (1), 26–37. https://doi.org/10.1017/qua.2018.12.
Tomkins, M.D., Huck, J.J., Dortch, J.M., Hughes, P.D., Kirbride, M.P., Barr, I.D., 2018b. b. Schmidt Hammer exposure dating (SHED): calibration procedures, new exposure age data and an online calculator. Quat. Geochronol. 44, 55–62. https://doi.org/10.1016/j.quageo.2017.12.003.
Thompson, A., Jones, A., 1986. Rates and causes of proglacial river terrace formation in southeast Iceland: an application of lichenometric dating techniques. Boreas 15 (3), 231–246. https://doi.org/10.1111/j.1502-3885.1986.tb00928.x.
Valet, J.-P., Meynadier, L., Guyodo, Y., 2005. Geomagnetic dipole strength and reversal rate over the past two million years. Nature 435, 802–805. https://doi.org/10.1038/nature03674.
Van der Veen, C.J., 1999. Fundamentals of Glacier Dynamics. Balkema, Rotterdam, p. 462.
Vargo, L.J., Anderson, B.M., Horgan, H.J., Mackintosh, A.N., Lorrey, A.M., Thornton, M., 2017. Using structure from motion photogrammetry to measure past glacier changes from historic aerial photographs. J. Glaciol. 63 (242), 1105–1118. https://doi.org/10.1017/jog.2017.79.
Viles, H., Goudie, A., Grab, S., Lalley, J., 2011. The use of the Schmidt Hammer and Equotip for rock hardness assessment in geomorphology and heritage science: a comparative analysis. Earth Surf. Process. Landforms 36 (3), 320–333. https://doi.org/10.1002/esp.2040.
Whalley, W.B., Douglas, G.R., Jonsson, A., 1983. The magnitude and frequency of large Rockslides in Iceland in the postglacial. Geogr. Ann. Phys. Geogr. 65, 99–110. https://doi.org/10.2307/520724.
Westoby, M.J., Brasington, J., J, Glasser, N.F., Hambrey, M.J. y, Reynolds, J.M., 2012. 'Structure-from-Motion' photogrammetry: a low-cost, effective tool for geoscience applications. Geomorphology 179, 300–314.
Wilson, P., Dunlop, P., Millar, C., Wilson, F.A., 2019. Age determination of glacially-transported boulders in Ireland and Scotland using Schmidt-hammer exposure-age dating (SHD) and terrestrial cosmogenic nuclide (TCN) exposure-age dating. Quat. Res. 92 (2), 570–582. https://doi.org/10.1017/qua.2019.12.
Wilson, P., Matthews, J.A., 2016. Age assessment and implications of late Quaternary periglacial and paraglacial landforms on Muckish Mountain, northwest Ireland, based on Schmidt-hammer exposure-age dating (SHD). Geomorphology 270, 134–144. https://doi.org/10.1016/j.geomorph.2016.07.002.
Wirz, V., Gruber, S., Purves, R.S., Beutel, J., Gärtner-Roer, I., Gubler, S., Vieli, A., 2016. Short-term velocity variations at three rock glaciers and their relationship with meteorological conditions. Earth Surf. Dyn. 4, 103–123. https://doi.org/10.5194/esurf-4-103-2016.